

Temporal Transfer Learning for Traffic Optimization with Coarse-Grained Advisory Autonomy

Jung-Hoon Cho, Sirui Li, Jeongyun Kim, Cathy Wu

Abstract—The recent development of connected and automated vehicle (CAV) technologies has spurred investigations to optimize dense urban traffic to maximize vehicle speed and throughput. This paper explores *advisory autonomy*, in which real-time driving advisories are issued to the human drivers, thus achieving near-term performance of automated vehicles. Due to the complexity of traffic systems, recent studies of coordinating CAVs have resorted to leveraging deep reinforcement learning (RL). Coarse-grained advisory is formalized as zero-order holds, and we consider a range of hold duration from 0.1 to 40 seconds. However, despite the similarity of the higher frequency tasks on CAVs, a direct application of deep RL fails to be generalized to advisory autonomy tasks. To overcome this, we utilize zero-shot transfer, training policies on a set of source tasks—specific traffic scenarios with designated hold durations—and then evaluating the efficacy of these policies on different target tasks. We introduce *Temporal Transfer Learning (TTL)* algorithms to select source tasks for zero-shot transfer, systematically leveraging the temporal structure to solve the full range of tasks. TTL selects the most suitable source tasks to maximize the performance of the range of tasks. We validate our algorithms on diverse mixed-traffic scenarios, demonstrating that TTL more reliably solves the tasks than baselines. This paper underscores the potential of coarse-grained advisory autonomy with TTL in traffic flow optimization.

Index Terms—Intelligent Transportation Systems, Learning and Adaptive Systems, Deep Learning in Robotics and Automation, Transfer Learning.

I. INTRODUCTION

THE recent advancements in connected and automated vehicle (CAV) technologies have opened up new frontiers in addressing the challenges of urban traffic congestion and associated environmental problems. The growing urgency to mitigate traffic-related issues, buoyed by advances in autonomous vehicles (AVs) and machine learning, is pushing the boundaries of urban roadway autonomy. As the transportation sector progressively moves towards a fully autonomous paradigm, the spotlight is firmly on devising innovative methods for traffic

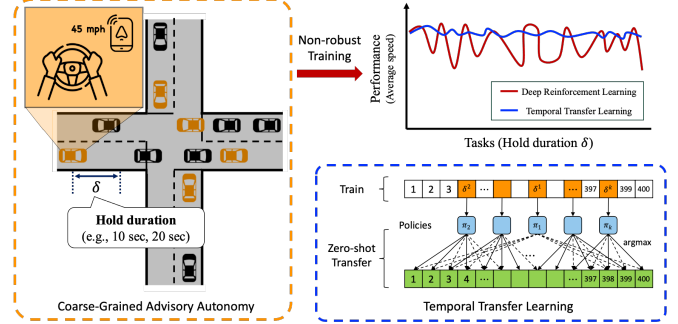


Fig. 1. Illustrative figure of Temporal Transfer Learning (TTL) for the coarse-grained advisory system. In a coarse-grained advisory system, vehicles receive persistent guidance for a specified hold duration rather than instantaneous controls. The system performance of this system shows the non-robustness to the hold duration of deep reinforcement learning when trained exhaustively. In that, we propose Temporal Transfer Learning (TTL) methods designed to select the source training tasks based on the temporal features. In comparison to the exhaustive and multi-task training methods, TTL gives an intermediate number of policies to train to solve a full set of tasks.

flow optimization, targeting key outcomes such as enhanced eco-driving, throughput maximization, and congestion reduction [1], [2].

This paper highlights the significant role of *advisory autonomy*, where real-time driving advisories are issued to human drivers to integrate seamlessly with other traffics and achieve better traffic flow. The crux of our research lies in demonstrating how advisory autonomy can enable human-driven vehicles to emulate the system-level performance of automated vehicles (AVs), providing a viable, cost-effective alternative in the near term. The notion of *coarse-grained advisory autonomy* is formalized through the lens of coarse-grained zero-order holds [3]. With this coarse-grained advice, instead of instantaneous controls ([4], [5], [6]), vehicles are provided with guidance that persists for a particular duration, thereby addressing the intricacies of fluctuating hold duration. This is significant as human drivers, unlike AVs, may find it challenging to adhere to frequent and rapid control changes. Specifically, our objective is to develop an algorithm that, given a traffic scenario, can determine whether guidance that human drivers could conceivably follow would achieve outcomes comparable to those of AVs. We concentrate on human compatibility for traffic optimization and the ability of human drivers to match corresponding system-level metrics (such as the average speed of all vehicles and the throughput) rather than achieve accurate maneuvers where AVs possess clear advantages, such as being able to react to abrupt braking without hesitation. This article subsumes and extends Sridhar *et al.* [3], which originally

Manuscript created in October 2023 and revised in May 2024.

Jung-Hoon Cho is with the Department of Civil and Environmental Engineering and the Laboratory for Information & Decision Systems, Massachusetts Institute of Technology, Cambridge, MA 02139, USA. (e-mail: jhooncho@mit.edu)

Sirui Li is with the Institute for Data, Systems, and Society and the Laboratory for Information & Decision Systems, Massachusetts Institute of Technology, Cambridge, MA 02139, USA. (e-mail: siruil@mit.edu)

Jeongyun Kim is with the Laboratory for Information & Decision Systems, Massachusetts Institute of Technology, Cambridge, MA 02139, USA. (e-mail: kji@mit.edu)

Cathy Wu is with the Laboratory for Information & Decision Systems; the Institute for Data, Systems, and Society; and the Department of Civil and Environmental Engineering, Massachusetts Institute of Technology, Cambridge, MA 02139, USA. (e-mail: cathywu@mit.edu)

formulated the problem as piecewise-constant control for traffic optimization. This paper further elaborates to include both acceleration and speed guidance and validate on different traffic networks.

Integrating this approach with reinforcement learning (RL) presents an elegant way forward, given RL’s structured framework for sequential decision-making. While deep RL has emerged as a potent tool for this purpose, its direct application to the advisory system has exposed a degree of fragility—characterized by jagged performance over a range of tasks, echoing the findings of Sridhar *et al.* [3]. This inconsistency and brittleness necessitate a more sophisticated approach to deep RL, one that can more reliably handle the complexities of real-world traffic scenarios encountered by advisory systems.

To confront these challenges head-on, we turned to transfer learning, a widely employed technique in numerous research fields that enables the utilization of knowledge acquired from one task to enhance performance in another related task [7], [8]. Specifically, transfer learning can be applied to adapt the pre-trained policy to a new task or to initialize a learning algorithm with pre-existing knowledge, substantially expediting the learning process and boosting overall performance. Transfer learning has been successfully applied to improve the efficiency and training performance of traffic management systems [9], [10], [4]. In this context, we employ zero-shot transfer, where policies are trained on a source task-specific traffic scenarios with designated hold duration—and then evaluated on different target tasks. This approach is computationally efficient as it obviates the need for any additional fine-tuning, directly leveraging the trained policies to new scenarios.

We introduce two *Temporal Transfer Learning* (TTL) algorithms—Greedy Temporal Transfer Learning (GTTL) and Coarse-to-fine Temporal Transfer Learning (CTTL). These algorithms adeptly leverage the temporal similarities across tasks to judiciously select training tasks, thereby significantly facilitating the training efficiency and overall performance. The essence of TTL lies in its capability to seamlessly transfer knowledge acquired from one task to another, circumventing the often observed training brittleness in deep RL algorithms. The TTL approach provides a structured advantage by systematically leveraging temporal structures inherent in the task domain. Our GTTL methods especially leverage a linear generalization gap which allows better navigation with fewer source trained models. This ability of TTL to draw insights from prior models offers a promising avenue to circumvent the fragility often observed in deep RL training. Then, to evaluate our algorithm’s generalizability, we consider validation on various traffic scenarios in which mixed-autonomy traffic has been proven effective for traffic optimization [5], [6].

The core contributions of this paper are twofold:

- We delve into a *coarse-grained advisory system*, presenting a compelling case for its viability in enhancing system-level traffic outcomes. Our empirical evidence underscores the possibility of furnishing human drivers with guidance that mirrors AV behavior, leading to tangible traffic improvements. Such findings pave the way

for considering human drivers as immediate, practical alternatives to full-fledged AV deployments.

- Our research introduces *Temporal Transfer Learning* (TTL) algorithms, a robust methodology specifically designed to tackle the training brittleness intrinsic to deep RL algorithms. TTL can be promising in evolving generalizable training paradigms for complex traffic optimization tasks by adeptly identifying sources of variation and harnessing insights from pre-existing models.

II. RELATED WORK

A. Reinforcement Learning for Mixed Autonomy Traffic

As we await the era of fully automated vehicles, we can anticipate a mixed autonomy system where automated and human-driven vehicles share the road. In such a system, controlling only a small proportion of the vehicles can significantly improve the overall traffic flow [5], [9]. Several studies have explored the potential of RL in addressing the challenges posed by the coexistence of AVs and human-driven vehicles. Researchers have worked on enhancing traffic efficiency in mixed autonomy settings using deep RL-based approaches and showed that it could eliminate stop-and-go traffic and congestion mitigation [5], [9], [2], [11], [4], [6]. These studies collectively highlight the potential of RL in optimizing mixed autonomy traffic, paving the way for enhanced safety, efficiency, and performance in transportation systems.

B. Advisory Autonomy

Advisory systems in roadway autonomy span a broad range of applications, from enhancing safety to mitigating traffic congestion. These systems provide considerable benefits to users. For instance, collision warning alerts have been employed to ensure the driver’s safety [12], and speed advisory systems at signalized intersections help users pass the green light efficiently [13]. At a system level, on the other hand, the advisory system provides system-level traffic optimization. For example, speed advisory systems contribute significantly towards eco-driving [14] and personalized advisory systems have been introduced to mitigate traffic congestion [15]. Furthermore, roadway signs suggesting advisory speeds represent another form of advisory autonomy.

However, the application of advisory systems poses unique challenges given their interaction with human drivers. While fully automated vehicles can operate within clearly defined parameters and constraints, human drivers behave differently. For instance, as noted by Mok *et al.*, humans require a minimum of 5-8 seconds to appropriately transition control [16]. This finding underscores the importance of accounting for the unique attributes and limitations of human drivers when developing control methods. For instance, Sridhar *et al.* identified two key characteristics of human-compatible driving policies: a simple action space and the capacity to maintain the same action for a few seconds [3]. An example of a human-compatible advisory system is a coarse-grained control system, which is provably stable in the context of Lyapunov in mitigating congestion on single-lane ring roads [17]. This system, known as an action-persistent Markov Decision Process

(MDP), successfully addresses the human need for simplicity and persistent actions. In light of these considerations, it is crucial to integrate human driving characteristics into the design of control methods for human drivers.

C. Action Persistent MDPs and RL

In exploring action repetition within reinforcement learning, the concept of Semi-Markov Decision Processes (Semi-MDPs) offers a rich framework for incorporating temporally abstract actions into the traditional MDP paradigm [18]. The ability to apply the same action across extended time periods allows for a simplified control strategy that can be beneficial for complex control problems.

Various methodologies such as reducing control granularity, implementing a skip policy, and applying temporal abstraction have been employed to analyze action repetition [19], [20], [21], [22]. Metelli *et al.* introduced action persistence and the Persistent Fitted Q-Iteration (PFQI) algorithm to modify control frequencies and learn optimal value functions [22]. Lee *et al.* addressed the multiple control frequency problems that guarantee convergence to an optimal solution and outperform baselines [23]. In the context of transportation systems, Sridhar and Wu investigate the use of piecewise constant policies for traffic congestion mitigation, providing a structured approach to guide human drivers in real-time [3].

These contributions collectively underscore the significance of action repetition and the strategic choice of control frequencies in RL. They also highlight the potential for translating these concepts into tangible traffic management solutions, exemplifying the intersection between theoretical research and practical application.

D. Transfer Learning in RL

Transfer learning is a popular technique used in various research domains to leverage the knowledge gained from one task to improve performance in another related task [7], [8]. In particular, transfer learning can be used to adapt a pre-trained policy to a new task or to initialize a learning algorithm with pre-existing knowledge, which can greatly accelerate the learning process and improve overall performance. In contrast to multitask learning's simultaneous approach, transfer learning applies knowledge from source tasks to optimize a particular target task, underscoring an asymmetrical relationship between tasks [8].

Transfer learning offers the advantage of significantly decreasing the amount of data needed for learning compared to traditional independent learning methods [24]. Dynamic transfer learning maps for multi-robot systems can be obtained by the basic system properties from approximated physical models or experiments [25]. Kouw and Loog not only delved into domain adaptation's specific instances and various techniques but also highlighted the challenges of sequential domain adaptation [26]. Moreover, transfer learning also has its benefit with the reduced number of data required for the new tasks coming from the shared representation of related tasks [24], [27], [28].

In robotics, transfer learning has been utilized for a wide range of applications such as robot manipulation, locomotion, and control [29], [30]. In the context of traffic settings, transfer learning has been applied to improve the efficiency and training performance of traffic management systems [9], [10], [4]. For example, Kreidieh *et al.* proposed a transfer learning framework that can help the warm start for training policies to dissipate shockwaves from closed traffic scenarios to more complex open ones [9]. Similarly, zero-shot policy transfer to adapt a pre-trained policy for autonomous driving in a structured environment to an unstructured environment results in improved performance and safety [10].

Also, the transferability of the learned policies may differ at different levels of tasks; for instance, policies derived from more structured and informative tasks are more robust to diverse tasks [31]. Yan *et al.* proposed a unified framework for traffic signal control using transfer learning to transfer knowledge across different intersections and adapt to varying traffic conditions [4]. Also, transfer learning is used for real-time crash prediction [32], and traffic flow prediction in data-sparse regions [33].

RL-based methods require generating significant amounts of simulation data, which can be costly. However, transfer learning offers a solution to alleviate the burden of data generation and simulation for training each model. By employing an efficient training scheme, the model can quickly learn when, what, and where to transfer knowledge in scenarios with limited data availability [34]. The selection of source tasks is critical in transfer learning as it sets the foundation for the efficacy of knowledge transfer. Contextual relevance in source task selection is critical in the efficacy that the transferability of a policy may be predicted through its relation to the target task's characteristics [35], [36]. Furthermore, Agostinelli *et al.* explore metrics that predict the success of transferred knowledge, facilitating the selection of source model ensembles to maximize performance on the target task [37]. In addition to selecting individual source tasks, multi-task learning can also be used to solve multiple related tasks [38].

A hierarchical approach to task granularity can be beneficial as it allows for the refinement of coarse attributes while learning more finer tasks. This method has been successfully employed by Wei *et al.* in their work on vehicle re-identification tasks [39] and in large-scale fault diagnosis tasks [40]. A coarse-to-fine framework can progressively improve task performance in complex problem-solving environments.

Overall, transfer learning has shown promising results in improving the efficiency and safety of traffic management systems by leveraging the similar temporal structure of a series of tasks and prior knowledge from related tasks.

III. PRELIMINARIES

A. Markov Decision Process and Reinforcement Learning

Markov Decision Process (MDP) is a mathematical process that models sequential decision-making problems. MDP is the 6-tuple $\mathcal{M} = (\mathcal{S}, \mathcal{A}, \mathcal{T}, \mathcal{R}, H, \gamma)$, where \mathcal{S} defines the state space, \mathcal{A} is action space, $\mathcal{T} : \mathcal{S} \times \mathcal{A} \times \mathcal{S} \rightarrow \mathbb{R}$ is a transition

probability distribution, \mathcal{R} is reward function, H is a total time horizon, and γ is a discount factor. The transition probability function $P(s'|s, a)$ specifies the probability of transitioning to a state s' from a state s by taking action a . An agent's objective in an MDP is to find a policy π that maximizes the expected sum of rewards obtained over time, given the current state s and the actions it can take.

Reinforcement learning (RL) is a subfield of machine learning that involves an agent learning to make a sequence of decisions by interacting with an environment. Since our problem setting for the advisory autonomy system is a sequential decision-making problem that can be formulated as MDP, RL chooses its actions based on the optimal policy to maximize the expected cumulative reward.

IV. COARSE-GRAINED CONTROL

A. Coarse-Grained Guidance in Advisory Autonomy

Advisory autonomy stands for the automated system that provides guidance to human drivers rather than a fully controllable process. In this context, it is designed to work in the presence of human-driven vehicles, ensuring that controlled vehicles operate in a manner that is safe, predictable, and intuitive for human drivers. *Coarse-grained control* refers to the vehicle control system that gives control periodically. Coarse-grained control involves applying the same action to an autonomous vehicle for a fixed time segment. As we discussed in Section II-C, coarse-grained control can be interpreted as an action persistent MDPs with different control granularities.

B. Action Persistent MDPs

We assume that all vehicles are human-driven vehicles. A subset of these vehicles, defined by the fraction ρ , receives periodic guidance from the advisory system and is termed *guided vehicles*. The remaining vehicles, constituting the fraction $(1 - \rho)$, are designated as *default-driven vehicles* and do not receive such guidance. Guided vehicles are human-driven vehicles with periodic assistance from a trained policy for coarse-grained control, $\pi_{\text{HC}}(s_{t_m})$. The policy is applied at intervals $t_m = \delta m$, where $m \in \mathbb{N}_0$ (\mathbb{N}_0 as a set of non-negative integers) and δ denotes the guidance hold duration. It's essential that the guidance hold duration is significantly shorter than the total horizon, denoted as ($H \gg \delta$). These vehicles receive guidance for any time t that falls within the range $[t_m, t_{m+1}]$. This action persistent MDP can be represented by the 7-tuple $\mathcal{M}_\delta = (\mathcal{S}, \mathcal{A}, \mathcal{T}, \mathcal{R}, H, \gamma, \delta)$.

Coarse-grained control, also known as piecewise constant control or zero-order hold control, refers to the application of the same control action over a specified time segment length [3]. In other words, the same action determined at time step t_m is applied to the time segment of $t \in [t_m, t_{m+1}]$. In the single-lane ring, the simulation experiments reported that the hold duration could be extended to 24 seconds without degradation of the system performance [3]. Li *et al.* derived sufficient conditions for piecewise-constant controls with the guidance hold duration to stabilize the system using the Lyapunov stability [17]. This piecewise constant control is backed up with the simulator experiments to evaluate the effect

of the coarse-grained advisory system [41]. Hasan *et al.* also introduces a cooperative advisory system that leverages a novel driver trait conditioned Personalized Residual Policy (PeRP) to guide drivers in ways that reduce traffic congestion [15].

C. Guidance Type

There are a few different ways to provide guidance to the guided vehicles. Based on the observation of the drivers, we can provide the drivers with either the target raw acceleration or target speed.

Acceleration Guidance. Acceleration guidance in advisory autonomy systems directs human drivers by recommending the optimal acceleration action, derived from a continuous set of possible actions according to the policy. This is represented by the function F_a , which determines the appropriate acceleration based on the current traffic state:

$$a_i(t) = F_a(s_i(t_k), \dot{s}_i(t_k), v_i(t_k)) \quad (1)$$

where $s_i(t)$ is a space headway between i th vehicle and the preceding vehicle, $v_i(t)$ is a velocity, and $a_i(t)$ is an acceleration of i th vehicle. This guidance applies for the duration $t \in [t_k, t_{k+1} = t_k + \delta]$.

For this acceleration guidance in the single-lane ring, Lyapunov analysis gives sufficient conditions for the stability of the coarse-grained advisory system [17]. Moreover, the success of this guidance system critically depends on the interface design through which advisories are communicated. A few challenges are possible discomfort for drivers, the complexity of human drivers in accurately interpreting and executing precise acceleration commands, and an increased risk of manual execution errors.

Speed Guidance. Speed guidance provides the autonomous vehicle with a discretized target speed, ensuring its attainment of the target speed as soon as possible while maintaining stability and adhering to preset boundaries. This approach is rooted in the challenges human drivers face in comprehending acceleration guidance [42]. Moreover, using acceleration guidance type for the coarse-grained control often struggles to achieve and sustain the optimal velocity as discussed in [43], [44].

Researchers have worked on the speed advisory system [45], [46], [47]. For example, Liang *et al.* guided the driver with the speed for signal phase and timing in CAV environment [45]. Wang *et al.* reported that the human-machine interface displaying the difference between current and suggested speeds with the cooperative driving simulator improved the performance while displaying time difference harmed the speed adaptation [48]. Speed guidance provides controlled human drivers with discretized target speeds and enforces them to reach these speeds as soon as possible, given the prevailing conditions. However, there are some drawbacks that human drivers tend to perceive the target speed as the easily broken speed limit and easily exceed the speed limit [49].

The speed guidance system provides the guided vehicle with the target speed of $v^*(t_k)$, which is represented by the

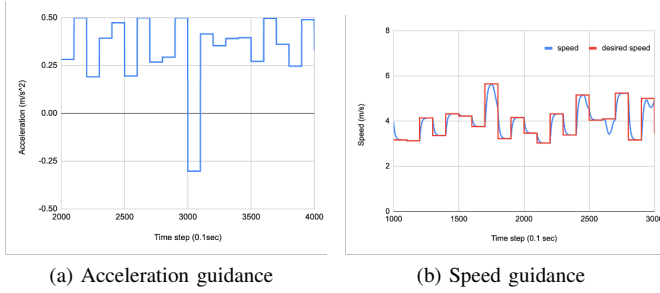


Fig. 2. Two types of advisory system to the human drivers: acceleration guidance (2a), speed guidance (2b).

function F_v . In control problems, the speed guidance takes the following form:

$$v^*(t_k) = F_v(s_1(t), \dot{s}_1(t), v_1(t)) \quad (2)$$

$$\dot{v}_i(t) = \alpha(v^*(t_k)) - v_1(t) + \beta\dot{s}_1(t) \quad (3)$$

This guidance applies for the duration $t \in [t_k, t_{k+1} = t_k + \delta]$.

Figure 2 intuitively depicts two distinct forms of advisory provided to drivers: acceleration and speed guidance. From a stabilization standpoint, speed guidance has certain advantages, as it allows the vehicle to sustain the same speed throughout the hold duration. However, under acceleration guidance, the vehicle’s speed is subject to change unless the acceleration is precisely zero. This inherent difference between the two forms of guidance leads to unique behaviors and responses in the traffic system, as demonstrated in our results.

V. TEMPORAL TRANSFER LEARNING

In advisory autonomy, we guide human drivers by providing a predetermined period, known as the hold duration, indicating how long they should maintain their guided actions. We consider solving families of MDP tasks whose only difference is the guidance hold duration since the control of humans can vary. That is, apart from this, all other traffic dynamics, such as the number of agents and road networks, remain completely identical. Even in this setting, we find that RL will train successfully in some scenarios and unsuccessfully in others, with no clear pattern among the tasks. Similar findings have been documented in [50].

The algorithm we introduce in this section is inspired by the intuition that an optimal strategy for hold duration δ should not be so different from that of hold duration $\delta' \approx \delta$. To see that this is especially true for small δ , consider that an optimal strategy under hold duration δ can be exactly recovered under the finer-grained control with the hold duration of $\delta/2$. We, therefore, exploit task similarity along the axis of hold duration to derive provably (sub)optimal strategies for transfer learning.

We wish to explore multiple tasks to understand the intricacies of the coarse-grained advisory system and its efficacy in optimizing traffic flow, particularly in mitigating congestion. Addressing multiple tasks gives us a holistic understanding of the system’s behavior under different scenarios, thus informing more robust optimization strategies. While solving multiple tasks simultaneously with a separate model per each task

TABLE I
TABLE OF NOTATIONS

Symbol	Description
δ	Guidance hold duration
$J(\delta)$	The performance of task with duration δ
A	The aggregate performance across different durations
k	Sequential step in source task selection
δ^k	The guidance hold duration chosen at k th step
π_k	The policy trained at the task at δ^k
$J^{\pi_k}(\delta^k)$	The performance of policy π_k evaluated at δ^k
$\Delta J(\delta_S, \delta_T)$	The generalization gap when the policy trained with δ_S transferred to the task with δ_T
$J_k(\delta)$	The performance updated with the best-performing performance among previously trained policies
S_k	A set of selected source tasks

could be computationally intensive and resource-demanding, leveraging a pre-trained model and transfer learning for our specific tasks can drastically reduce the computational burden. This strategy not only saves valuable time but also harnesses the knowledge from the pre-trained model to achieve superior performance. Thus, it is crucial to design a systematic approach for transfer learning to make the process efficient and effective. Focusing on the hold duration, we observe three main properties regarding the relationship between the tasks: estimated performance, upper-bound performance, and generalization gap. The list of variables and functions used throughout this paper is summarized in the Table I, ensuring clarity and ease of reference for the reader.

A. Problem Definitions

Guidance Hold Duration and Performance. In coarse-grained advisory settings, we denote the *performance* of the task with a hold duration of δ as $J(\delta)$. The guidance hold duration δ can range from a minimum value (δ_{\min}) to a maximum value (δ_{\max}).

The *aggregate performance* $A(\delta_{\min}, \delta_{\max})$ is the continuous integral of the estimated performance function over a range of guidance hold duration, providing a measure of system performance across different durations.

$$A(\delta_{\min}, \delta_{\max}) = \int_{\delta_{\min}}^{\delta_{\max}} J(\delta) d\delta \quad (4)$$

This involves calculating the area under the curve that the performance function $J(\delta)$ describes. In the empirical sections of this paper, we will use this discrete summation instead of a continuous integral for simplicity. We denote the discrete sum of estimated performance over a range of δ as $\tilde{A}(\delta_{\min}, \delta_{\max}) = \sum_{\delta=\delta_{\min}}^{\delta_{\max}} J(\delta)$. For notational convenience, we will henceforth denote $A(\delta_{\min}, \delta_{\max})$ by A .

Sequential source tasks selection problem. We define the *sequential source tasks selection problem* which is sequential optimization problem of selecting the next source training task that maximizes the estimated performance of the set of trained policies. It is worth noting that, in the sequential source task selection problem, selecting the task expected to yield the greatest marginal improvement in estimated performance is equivalent to choosing the one that maximizes overall aggregated performance. We employ k to represent the k th

source task training, while K denotes the transfer budget, the maximum limit of such iterations. For the initial selection of the source task, we train the policy for the MDP task, which is associated with δ^1 . Any subsequent selection iteration, marked as k , involves the policy’s training for tasks related to δ^k . We denote a set of selected source tasks at k th iteration as S_k . We also define $J_k(\delta)$ as the estimated performance of a task with the hold duration of δ after k iterations. When training the model for an MDP with a hold duration of δ^k , we obtain the policy π_k , and its performance at the task with δ^k is $J^{\pi_k}(\delta^k)$. Solving the source task selection problem greedily at every iteration can be equivalent to selecting the task that maximizes the estimated area. The trajectory of transfer tasks from δ^1 to δ^K reflects tasks trained along the transfer steps.

We initialize the estimated performance $J_0(\delta)$ for all guidance hold durations δ within the range of interest to zero, which sets the baseline for subsequent improvements:

$$J_0(\delta) = 0 \quad \forall \delta \in [\delta_{\min}, \delta_{\max}]. \quad (5)$$

As we iterate through the process of selecting source tasks, we account for the possibility that a policy trained on one task may not perform optimally when applied to a different task without retraining, known as the *generalization gap*. This concept captures the decline in performance when a policy trained for a source task δ_S is applied, without modification, to a related yet different target task δ_T . Such performance degradation in performance has been studied in literature [51], [52], and similar effects have been observed in multi-objective contexts [53]. The generalization gap is crucial for understanding the limits of transfer and for guiding the iterative improvement of task-specific policies in reinforcement learning.

Definition 1 (Generalization gap $\Delta J(\delta_S, \delta_T)$). *The generalization gap quantifies the expected reduction in performance when a policy, originally optimized for a source task with hold duration δ_S , is transferred to a target task with duration δ_T . The gap $\Delta J(\delta_S, \delta_T)$ is defined as the difference between the performance at the source task, $J(\delta_S)$, and the estimated performance when applied to the target task.*

Each iteration k updates the estimated performance $J_k(\delta)$ by incorporating the highest performing policy thus far. For a task with hold duration δ^k , this update is formalized as follows:

$$J_k(\delta) = \begin{cases} J^{\pi_k}(\delta^k), & \text{if } \delta = \delta^k \\ \max(J_{k-1}(\delta), J^{\pi_k}(\delta^k) - \Delta J(\delta^k, \delta)), & \text{otherwise.} \end{cases} \quad (6)$$

This ensures that at any given step, the system leverages the best-available knowledge from the training of policies across varying tasks, thereby iteratively enhancing the overall performance landscape.

Definition 2 (Sequential Source Tasks Selection Problem). *The Sequential Source Tasks Selection Problem aims to sequentially identify the optimal guidance hold duration δ^k that maximizes the estimated performance of a trained policy. Specifically:*

- For the initial step ($k = 1$), select any δ^1 from the specified range of durations.

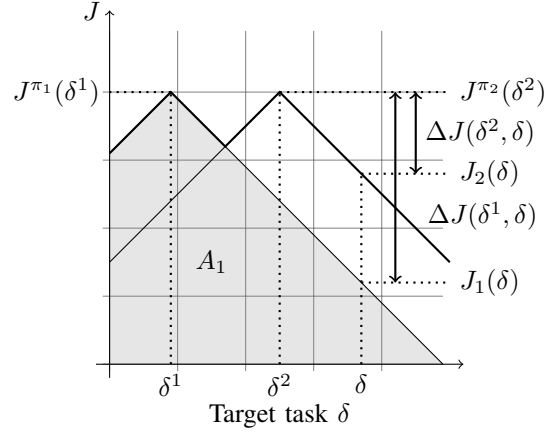


Fig. 3. Visualization of sequential source task selection and corresponding performance evaluations within the guidance hold duration space. The shaded region represents the aggregate performance A_1 after selecting δ^1 in the first step. The generalization gap $\Delta J(\delta^1, \delta)$ quantifies the performance drop when applying the policy trained at δ^1 to a target task with δ . At the second step, the selection of δ^2 updates the estimated performance of task with duration of δ from $J_1(\delta)$ to $J_2(\delta)$.

- For each subsequent step ($k = 2, \dots, K$), δ^k is chosen to maximize the aggregate estimated performance A_k , formulated as:

$$\delta^k = \arg \max_{\delta} A_k, \quad (7)$$

where the aggregate performance A_k is the integral of the performance function $J_k(\delta)$ over the guidance duration interval $[\delta_{\min}, \delta_{\max}]$:

$$A_k = \int_{\delta_{\min}}^{\delta_{\max}} J_k(\delta) d\delta. \quad (8)$$

This optimization progresses iteratively, enhancing policy performance with each selected task.

Figure 3 presents a conceptual visualization of the sequential source task selection process and the associated generalization gaps encountered during zero-shot policy transfer. The generalization gap $\Delta J(\delta^1, \delta)$ reflects the performance decrement when the policy, initially trained at δ^1 , is applied to a target task with guidance hold duration δ . Subsequent selections of source tasks, such as δ^2 , further improve the estimated performance across different task durations.

B. Modeling Assumptions

In this section, we delineate our assumptions for the development of our algorithm for source tasks selection problem. These assumptions enable us to formalize the temporal transfer learning systematically.

Assumption 1 (Constant upper-bound performance). *The upper bound performance of $J^*(\delta)$ remains constant across all guidance hold duration δ within the range $[\delta_{\min}, \delta_{\max}]$, symbolized as:*

$$J^*(\delta) = J^* \quad \forall \delta \in [\delta_{\min}, \delta_{\max}]. \quad (9)$$

Assumption 1 is supported by empirical analysis within coarse-grained advisory autonomy settings, suggesting that various coarse-grained guidance tasks may uphold the same upper-bound performance. Our observations in single-lane ring environments validate this assumption (Figure 9a), although it is noted that in more complex scenarios like highway ramps, the upper-bound performance may decline as hold duration increases (Figure 9b).

Assumption 2 (Deterministic training performance). *For any task trained with hold duration δ^k , the achieved performance consistently matches the upper bound of $J^*(\delta^k)$, represented as:*

$$J^{\pi_k}(\delta^k) = J^*(\delta^k). \quad (10)$$

Assumption 1 and 2 imply that the selected task training leads directly to achieving the theoretical upper-bound performance, assuming optimal training conditions.

Assumption 3 (Linear generalization gap). *The generalization gap $\Delta J(\delta_S, \delta_T)$ between transferring from a source hold duration δ_S to a target hold duration δ_T is linearly related to the absolute difference between δ_S and δ_T , as follows:*

$$\Delta J(\delta_S, \delta_T) = \begin{cases} \theta_L(\delta_S - \delta_T), & \text{if } \delta_S > \delta_T \\ \theta_R(\delta_T - \delta_S), & \text{otherwise} \end{cases} \quad (11)$$

where θ_L signifies the slope of transfer performance when transitioning from a coarser to a finer task, implying that $\delta_S > \delta_T$. Conversely, θ_R represents the slope when shifting from a finer to a coarser task, suggesting that $\delta_S < \delta_T$.

Assumption 4 (Symmetric generalization gap function). *The degradation rates, whether transitioning from a coarse to a fine task or vice versa, are the same, which is formalized as:*

$$\theta_L = \theta_R \quad (= \theta). \quad (12)$$

Assumption 4 simplifies the analysis by asserting that the granularity of the task does not influence the rate of performance degradation during policy transfer.

Assumption 5 (Bounded slope of generalization gap function). *The upper-bound performance J^* is assumed to be greater than or equal to $\theta(\delta_{\max} - \delta_{\min})$, implying the slope of the generalization gap function is less than or equal to $\frac{J^*}{\delta_{\max} - \delta_{\min}}$.*

$$\theta \leq \frac{J^*}{\delta_{\max} - \delta_{\min}} \quad (13)$$

Assumption 5 establishes a boundary for the slope of the generalization gap function relative to the range of hold durations, facilitating the interpretability of geometric analysis. If J^* is larger than $\theta(\delta_{\max} - \delta_{\min})$, the transfer from any point would be able to encompass the additional volume. Thus, without loss of generality, we can assume $J^* = \theta(\delta_{\max} - \delta_{\min})$ in our geometric analysis. If J^* is less than $\theta(\delta_{\max} - \delta_{\min})$, indicating a relatively constrained effective transfer range, the advantage of using transfer learning might be limited. This is

due to the fact that TTL tends to benefit from the case where the amount of generalization gap is prominent.

C. Optimal Strategy for Source Tasks Selection Problem

With several assumptions we made in the previous section, we can devise a systematic algorithm to solve the source tasks selection problem and choose the subsequent training source task based on the simple geometry. We consider analysis that simplifies the marginal performance improvement after each iteration to obtain intuition and provide a theoretical grounding for the TTL process.

As demonstrated in Figure 3 and supported by Assumptions assumption 1, assumption 2, and 3, training on the source task selected at each decision round achieves optimal performance and results in the emergence of two distinct segments. These segments, delineated by the chosen source task, can be accurately modeled using piecewise linear functions. After $(k - 1)$ iterations of selecting source task, there will be k distinct segments with inflection points at $\delta^1, \dots, \delta^{k-1}$ as illustrated in Figure 4. This segmentation helps the following analyses, identifying segments with the largest increase in aggregate performance. Our objective is to find the next δ^k that maximizes the A_k . To achieve this, we systematically evaluate each of these small piecewise linear segments. For each segment, we calculate the potential marginal increase in A_k . The specific marginal increase for each segment is influenced by the underlying shape of the performance function J .

Figure 4 illustrates different decision rules about where to transfer and how much area to be covered based on the $J(\delta)$ shape. Decision rules for TTL are based on the assumptions we made to simplify the analysis. Assumption 1 assumes the upper bound performance J^* to be the flat shape as a blue dotted line, Assumption 3 and Assumption 4 makes the transfer performance functions in both directions have linear functions with an identical slope.

We present Theorem 1 grounded on the geometric characteristics of the function $J(\delta)$ and the estimated marginal increase in A_k . This theorem embodies a greedy strategy for the source tasks selection problem. It aims to assess the estimated marginal increase in performance across each piecewise linear segment, choosing the optimal subsequent transfer task of δ^k within the designated segment. The term ‘‘greedy’’ is chosen as it focuses only a single step look-ahead at any given instance. The greedy optimal strategy for optimal transfer to maximize the estimated performance of the policy is to choose the piecewise linear segment estimated to increase by the largest area.

Theorem 1 (Optimal source task selection for greedy transfer). *Given a restricted piecewise linear segment of $J_k(\delta)$ with the longest length of δ segment such that $\delta \in [\delta_L, \delta_R]$, the greedy policy for choosing the optimal transfer target, δ^k , to maximize the estimated aggregate performance, as:*

$$\delta^k = \begin{cases} \frac{\delta_L + \delta_R}{2} & \text{for } k = 1 \text{ or } J_k \text{ symmetric} \\ \frac{2\delta_L + \delta_R}{3} & \text{for } k \neq 1 \text{ and } \frac{dJ_k}{d\delta} > 0 \\ \frac{\delta_L + 2\delta_R}{3} & \text{for } k \neq 1 \text{ and } \frac{dJ_k}{d\delta} < 0 \end{cases} \quad (14)$$

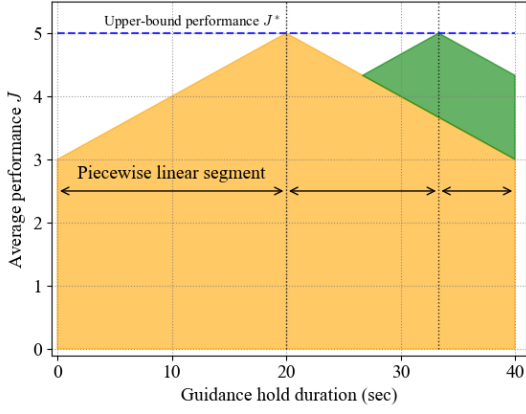


Fig. 4. An exemplified representation of the Temporal Transfer Learning (TTL) process for source task selection. The graphic showcases the stepwise procedure for two iterations ($k = 2$), resulting in two segments demarcated by inflection points at δ^1 and δ^2 . The upper-bound performance J^* is indicated by the blue dotted line, as posited in assumption 1, while the piecewise linear segments and their slopes, as governed by assumption 3 and 4, guide the selection of the next hold duration δ^k that will maximize the aggregate performance A_k . Each segment is assessed for its potential marginal contribution to A_k , with decisions influenced by the shape of the performance function $J(\delta)$, here visualized as transitions from the orange to the green area, signifying the shift in guidance hold duration from $\delta^1 = 20$ to $\delta^2 = 33.33$.

Utilizing this selection strategy, the estimated marginal increase in aggregate performance A_k can be computed along the given range of segments, taking into account the curvature of J :

$$\Delta A_k = \begin{cases} \frac{3}{4}\theta(\delta_R - \delta_L)^2 & \text{for } k = 1 \\ \frac{1}{8}\theta(\delta_R - \delta_L)^2 & \text{for } k \neq 1 \text{ and } J_k \text{ symmetric} \\ \frac{1}{3}\theta(\delta_R - \delta_L)^2 & \text{otherwise.} \end{cases} \quad (15)$$

In Appendix A, we provide detailed proofs for Theorem 1, based on the underlying geometric shape of both the estimated performance and its aggregate.

We can devise a greedy, efficient, and robust algorithm for temporal transfer learning by leveraging the aforementioned assumptions and the estimated performance function. We present *Greedy Temporal Transfer Learning (GTTL)* algorithm (Algorithm 1), an iterative system that determines which task of hold duration to transfer at each iteration. Given the estimated performance function, we have the capability to choose the most advantageous initial training point. With the Assumption 4, intuitively, the point that maximizes the estimated covered area along the ranges is the median within the entire range of hold duration. For the subsequent decisions, we choose the best option based on the Theorem 1. The transfer process continues until the area is sufficiently covered or once the number of source tasks exceed the predefined transfer budget, in case we have it. Figure 5 describes the difference between TTL algorithms in the coherent transfer procedure between temporally linked tasks.

Algorithm 1 starts by initializing with the minimum and maximum hold duration, setting the performance of all hold

Algorithm 1 Greedy Temporal Transfer Learning (GTTL)

Input: MDP $\mathcal{M}(\delta)$, Hold duration range $[\delta_{\min}, \delta_{\max}]$, Upper bound area A^* , Termination criteria ε , Transfer budget K

Output: J_k and S_k

Initialize : $J_0(\delta) = 0 \forall \delta \in [\delta_{\min}, \delta_{\max}]$, $A_k = 0$, $S_k = \{\}$, $\pi = \{\}$, $k = 0$

- 1: **while** ($A_k \leq (1 - \varepsilon)A^*$) and ($k \leq K$) **do**
- 2: $\delta^{k+1} \leftarrow$ **FindGreedyTransferPoint**($S_k, J_k, \delta_{\min}, \delta_{\max}$)
- 3: $S_{k+1} \leftarrow S_k \cup \{\delta^{k+1}\}$
- 4: $\pi_{k+1} \leftarrow$ **Train**($\mathcal{M}(\delta^{k+1})$)
- 5: $\pi \leftarrow \pi \cup \{\pi_{k+1}\}$
- 6: $J_{k+1}(\delta^{k+1}) \leftarrow J^{\pi_{k+1}}(\delta^{k+1})$
- 7: $J_{k+1}(\delta) \leftarrow \max(J_k(\delta), J_{k+1}(\delta^{k+1}) - \Delta J(\delta^{k+1}, \delta))$
 $\forall \delta \in (\delta_{\min}, \delta_{\max}) \setminus \delta^{k+1}$
- 8: $A_{k+1} = \int_{\delta_{\min}}^{\delta_{\max}} J_{k+1}(\delta) d\delta$
- 9: $k \leftarrow k + 1$
- 10: **end while**
- 11: **return** J_k and S_k

Algorithm 2 Find Greedy Transfer Point

Function FindGreedyTransferPoint($S_k, J_k, \delta_{\min}, \delta_{\max}$)

- 1: Cut a range of hold duration $[\delta_{\min}, \delta_{\max}]$ into the segments split by $\delta^k \in S_k$
- 2: // Choose δ^k within the segment of $[\delta_L, \delta_R]$ based on the slope of J_k (Theorem 1)
- 3: **if** J_k is symmetric **then**
- 4: $\delta^k \leftarrow \frac{\delta_L + \delta_R}{2}$
- 5: **else if** J_k has positive slope **then**
- 6: $\delta^k \leftarrow \frac{2\delta_L + \delta_R}{3}$
- 7: **else if** J_k has negative slope **then**
- 8: $\delta^k \leftarrow \frac{\delta_L + 2\delta_R}{3}$
- 9: **end if**
- 10: **return** δ^k

duration to 0, initializing J and S to 0, and having an empty set for the policies. It continues as long as the covered area is below a threshold or the number of source tasks is less than the budget. For simplicity in notation, we propose substituting the whole area of $(\delta_{\max} - \delta_{\min})J^*$ with A^* . Inside the loop, the algorithm chooses a new training task with a hold duration of δ^{k+1} and appends it to its set. It then trains a policy for this hold duration and adds it to the set of policies. After updating the performance with this new policy, the algorithm then calculates the area under this performance curve. Once the loop finishes, the algorithm returns the best performance for each task (J_k) and a set of selected training tasks (S_k). In Algorithm 1, Algorithm 2 assists in identifying the greedy training source task, drawing insights from the shape of the estimated performance function J . This decision-making rule is grounded in Theorem 1.

GTTL algorithm (Algorithm 1) exhibits several noteworthy characteristics underpinning its functionality and efficiency. This algorithm is formulated as an anytime algorithm, meaning it can provide a valid solution even if stopped in the middle of the iterations. Beyond mere validity, GTTL algorithm offers performance assurances. At any given step k , GTTL not only

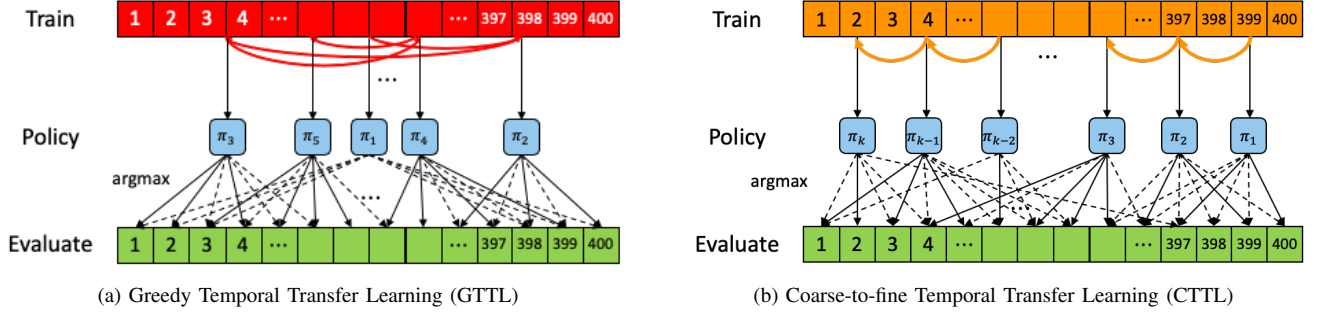


Fig. 5. **Illustrative figure of Temporal Transfer Learning (TTL) algorithms:** Selecting the training task based on the TTL algorithm, evaluating each task based on the trained policies, and taking the best-performing policy for each task.

provides a valid solution but also ensures a performance that is oriented towards optimization. For example, CTTL might struggle with finer tasks in the initial selection of the source task. This is because the trained policy is inherently skewed to excel in coarser tasks. This means that while other methods like CTTL can also deliver valid results at step k , GTTL is specifically designed to offer a performance closer to optimal at every individual step. This property ensures flexibility and usability under varying operational constraints, allowing continuous solution improvement with each additional source task. This intelligent selection process ensures efficient knowledge transfer and promotes effective learning across different stages of the algorithm’s execution.

D. Theoretical Analysis for Optimal Temporal Transfer Learning

The next natural question is how good are these incremental transfer learning strategies over multiple iterations of selecting source tasks. The optimality criterion can be defined as the best performance achieved within K steps. Until now, we have focused on the performance we could achieve with the number of steps. Drawing an analogy to K-means clustering, the predetermined number of source tasks of K in CTTL resembles the predefined number of clusters in K-means, which can often be a limitation if not chosen wisely, as it directly influences the granularity of the solutions and potentially the computational budget. Thus, in practice, where training computation budgets are constrained, we care about the dual of this. Moreover, the dual optimality criterion could be how many source tasks are needed to achieve a certain performance threshold. We can analyze the number of steps $K^*(\epsilon)$ that can achieve some given suboptimality ϵ . This measure provides a quantifiable way to evaluate the algorithm’s efficiency and effectiveness in traversing the solution space, adding another layer of flexibility and adaptability to its application.

Definition 3 (Cumulative area under the estimated performance function at each iteration). *For each successive iteration of selecting source task, denoted as k , the trained model’s cumulative area under the estimated performance function at the k th iteration is represented as A_k . $K^*(\epsilon)$ is an optimal K to be the discrete sum of estimated performance to have*

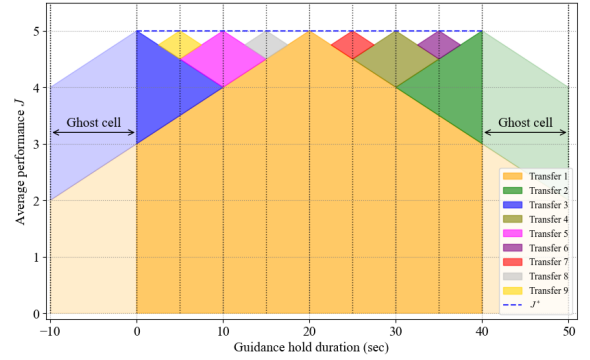


Fig. 6. Illustrative figure for the *lower bound of Greedy Temporal Transfer Learning (GTTL)* with the ghost cells at the end of the segments.

suboptimality of ϵ . This relationship can be formally defined through the following equations:

$$A_{K^*(\epsilon)} \geq (1 - \epsilon)A^* \quad (16)$$

As we progress further, the cumulative gain A_k inches closer to the maximum possible performance J^* , indicating that the performance coverage improves with the additional policy obtained by training the source task. However, the speed of improvement depends on the specifics of the generalization gap and the range of guidance hold duration. Definition 3 essentially conveys about the optimal K (K^*) that is estimated to cover the area of $(1 - \epsilon)A^*$, having remaining area represented by the ratio of ϵ . Hence, the definition offers insight into how many steps are required to meet the prespecified level of performance as we iterate. These equations also provide a quantitative understanding of how performance coverage evolves with each iteration and how close it gets to the maximum possible performance. At every iteration, it is crucial to consider the potential coverage area of each monotonic segment. However, it is hard to write a clean, closed-form solution for the optimal policy because the segments on the sides have different shapes from the others when choosing the largest section.

To have a clean, closed-form analysis, the lower bound performance of GTTL is given by creating ghost cells at the end of the whole segment as depicted in Figure 6. This lower-

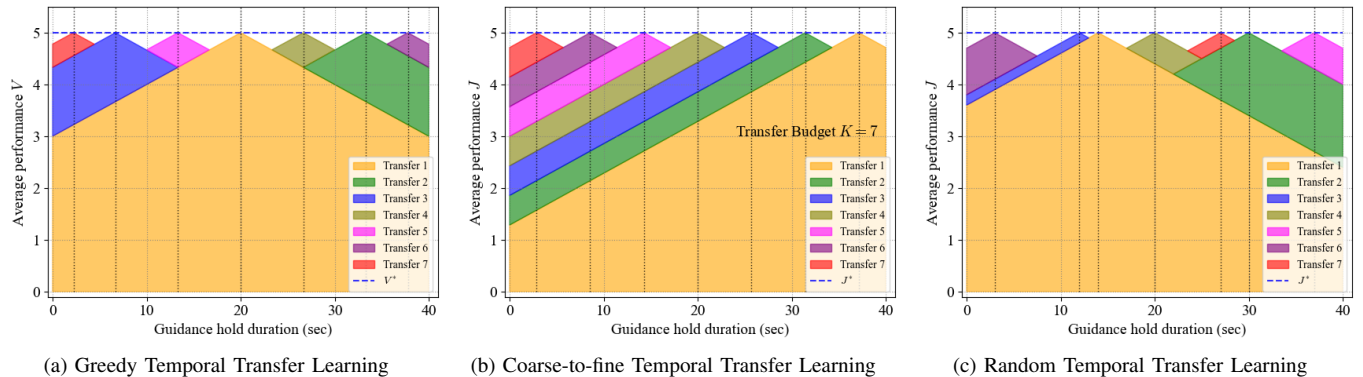


Fig. 7. Illustrative figures for comparing marginal area increase at each iteration by Greedy Temporal Transfer Learning (GTTL), Coarse-to-fine Temporal Transfer Learning (CTTL) for a given budget K , and Random Temporal Transfer Learning (RTTL).

bound case chooses δ_{\max} and δ_{\min} for the second and third selection of source tasks, respectively, to create the symmetric V-shaped estimated performance for all sub-segments. This idea enables us to simplify the evaluation process while maintaining reasonable accuracy. The lower bound of the cumulative area of GTTL up to iteration k is represented by \tilde{A}_k .

Lemma 2 (Lower bound of Greedy Temporal Transfer Learning). *At each step, A_k is always greater or equal to \tilde{A}_k .*

$$A_k \geq \tilde{A}_k \quad \forall k = 1, \dots, K \quad (17)$$

Proof. It is important to note that \tilde{A}_k will always be less than or equal to A_k , which represent the cumulative areas under the estimated performance function. This discrepancy arises because the GTTL consistently chooses the optimal task to maximize the area at each step, while \tilde{A}_k opts for sub-optimal choices of the second and third source tasks. \square

Theorem 3 highlights that if there exists an integer n such that \tilde{A}_n is greater than or equal to $(1 - \varepsilon)A^*$, then it logically follows that the cumulative area under the entire value function A_n is also greater than or equal to $(1 - \varepsilon)A^*$. This is grounded by its definition that A_n is never less than \tilde{A}_n .

Theorem 3 (The number of source tasks required to cover the area). *Given an integer n for which $\tilde{A}_n \geq (1 - \varepsilon)A^*$, it is demonstrable that $A_n \geq (1 - \varepsilon)A^*$ because $A_n \geq \tilde{A}_n$. Also, we require at least $\frac{4\varepsilon+1}{4\varepsilon}$ steps to cover at least $(1 - \varepsilon)A^*$.*

We prove Theorem 3 by leveraging the lower bound cumulative area of GTTL as outlined in Lemma 2, which has a streamlined expression of A_n . The comprehensive proof is provided in Appendix B.

E. Bounded Suboptimality

If we have privileged access to the transfer budget, we can devise a better algorithm than GTTL, since GTTL can be viewed as decision-making based on a 1-step greedy policy. This motivates us to introduce the *Coarse-to-fine Temporal Transfer Learning (CTTL)*, a structured and sequential way

of transferring. The algorithm systematically selects steps that span the task range uniformly for a given set number of source tasks. Initiation occurs with the coarser tasks, progressively narrowing down to the finer ones. For example, given the budget of source tasks of 7 and a hold duration range from 1 to 40, the training begins with a hold duration of 37.14 and subsequently transitions to 31.43, 25.71, 20, 14.29, 8.57, and then 2.86, mirroring a diminishing granularity (Figure 7b).

The inherent advantage of starting with coarser tasks is their limited effective horizon, simplifying their resolution. Consequently, they often pose fewer challenges compared to their finer counterparts. Moreover, existing literature suggests that a coarse-to-fine temporal transfer learning approach can be advantageous, particularly when adapting a pre-trained policy from a coarser to a finer task [39], [40].

Algorithm 3 Coarse-to-fine Temporal Transfer Learning (CTTL)

Input: MDP $\mathcal{M}(\delta)$, Range of hold duration $[\delta_{\min}, \delta_{\max}]$, Transfer budget K

Output: J_k and S_k

Initialize : $J_0(\delta) = 0 \quad \forall \delta \in [\delta_{\min}, \delta_{\max}]$, $S_k = \{\}$, $\pi = \{\}$, $k = 0$

- 1: **while** $k \leq K$ **do**
 - 2: $\delta^{k+1} = \delta_{\max} - \frac{2k+1}{2K}(\delta_{\max} - \delta_{\min})$
 - 3: $S_{k+1} \leftarrow S_k \cup \{\delta^{k+1}\}$
 - 4: $\pi_{k+1} \leftarrow \text{Train}(\mathcal{M}(\delta^{k+1}))$
 - 5: $\pi \leftarrow \pi \cup \{\pi_{k+1}\}$
 - 6: $J_{k+1}(\delta^{k+1}) \leftarrow J^{\pi_{k+1}}(\delta^{k+1})$
 - 7: $J_{k+1}(\delta) \leftarrow \max(J_k(\delta), J_{k+1}(\delta^{k+1}) - J_{\delta^{k+1} \rightarrow \delta})$
 $\quad \quad \quad \forall \delta \in (\delta_{\min}, \delta_{\max}) \setminus \delta^{k+1}$
 - 8: $k \leftarrow k + 1$
 - 9: **end while**
 - 10: **return** J_k and S_k
-

Lemma 4 states the optimality of the CTTL algorithm, which selects its subsequent transfer task contingent on the allocated transfer budget K . Algorithm 3 establishes a structured, sequential framework for transitioning from coarser to finer tasks across specified iterations. Given a range of hold durations and a budget K , it begins with a coarser task and

gradually advances to finer tasks, ensuring that each iteration spans the task range uniformly.

Lemma 4 (Optimality of Coarse-to-fine Temporal Transfer Learning). *Coarse-to-fine Temporal Transfer Learning (CTTL) algorithm optimizes maximizing the cumulative area under the performance function given the transfer budget of K under assumptions 1, 3, 4, and 5. Initiated from the coarsest task with the hold duration of $(\delta_{max} - \frac{\delta_{max} - \delta_{min}}{2K})$, CTTL progressively transitions to finer tasks, each marked by an equidistant progression of $(\frac{\delta_{max} - \delta_{min}}{K})$. The optimal estimated performance of CTTL after K iterations is written as follows:*

$$A_K^{CTTL} = (1 - \frac{1}{4K})\theta(\delta_{max} - \delta_{min})^2 \quad (18)$$

The optimality of CTTL can be proved by the equality condition of the Cauchy-Schwarz inequality. The authors may recommend readers to go through the detailed proof in Appendix C.

Notably, when one possesses an intimate knowledge of the number of source tasks $K^*(\epsilon)$, CTTL tends to outpace the GTTL algorithm. However, obtaining such precise information on the transfer budget remains a challenge in practice. Therefore, it is crucial to analyze the degree to which GTTL might be suboptimal compared to the oracle-like CTTL. In essence, we seek to quantify the suboptimality gap between the two. Theorem 5 contends the suboptimality and its bound of GTTL compared to CTTL, given that CTTL achieves the optimal strategy with the transfer budget of K .

Theorem 5 (Suboptimality of Greedy Temporal Transfer Learning). *GTTL operates at a suboptimal level relative to CTTL, bounded by:*

$$\begin{cases} \frac{1}{4K(K-1)}\theta(\delta_{max} - \delta_{min})^2 & \text{for } K = 2^i + 1 \\ \frac{1}{2(K-1)^2}\theta(\delta_{max} - \delta_{min})^2 & \text{otherwise} \end{cases} \quad (19)$$

where $i \in \mathbb{N}_0$.

The proof for Theorem 5 is detailed in Appendix D, where the suboptimality bounds of GTTL relative to CTTL are expounded, specifically for two distinct cases dictated by the value of K . The proof is grounded in the algebraic elucidation of this suboptimality measure.

VI. SIMULATION EXPERIMENTS

This section elucidates the simulation experiments conducted to address our primary research questions. The main purpose of our investigation is to explore the potential of human-compatible control serving as an immediate surrogate for AVs and to verify the degree to which such control can optimize traffic performance at a system level. We conducted many experimental trials in various environments to obtain valuable answers to these essential questions.

A. Modular Road Networks

In mixed-autonomy roadway settings, we delve into various traffic scenarios as explored in prior works [4], [5], [6], including single-lane ring, highway ramp, and signalized intersection

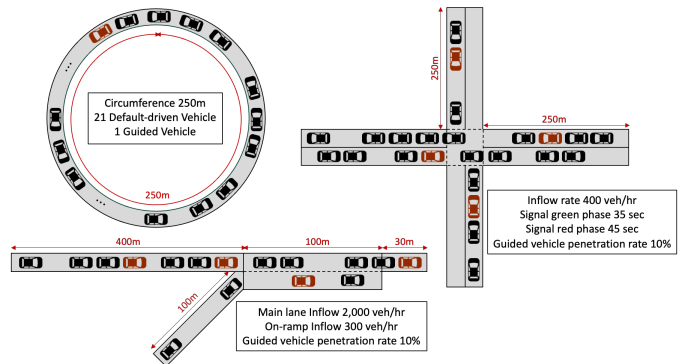


Fig. 8. **Modular road networks.** Three traffic scenarios for mixed autonomy roadway settings: single-lane ring (top left), highway ramp (bottom), and signalized intersection (top right).

networks, as depicted in Figure 8. Each scenario has distinct objectives; for instance, the single-lane ring and intersection aim to elevate all vehicles' average velocity, while the highway ramp scenario focuses on increasing the outflow given a constant inflow. On the other hand, the signalized intersection scenario employs a multitask RL strategy, simulating varied penetration rates to accommodate different levels of human-guided vehicle presence, with an evaluation of a penetration rate of 0.1 to assess the RL policy's performance. Default-driven vehicles, which are not equipped with the guidance system, adhere to the Intelligent Driver Model (IDM) for car-following [54].

In the single-lane scenario, the state space is defined by the ego vehicle's speed, the leading vehicle's speed, and the headway. For the highway ramp scenario, the state includes the ego vehicle's speed, relative positions and speeds of the leading and following vehicles in the same lane, and those of the following vehicle on the ramp. In the intersection scenario, the state comprises the ego vehicle's speed, the distance remaining to the intersection, the traffic signal phase, as well as the relative positions and speeds of the leading, following, and adjacent vehicles, the current speed limit, and lane and road identifiers.

The action space varies with the type of guidance employed. For acceleration guidance, a continuous action space ranging from -1 to 1 is utilized, directly influencing the vehicle's acceleration up to a capacity of 2.5m/s^2 . On the other hand, for speed guidance, a discrete action space is defined, with ten actions ranging from 0 to 1 , where the chosen action is scaled by the speed limit to determine the vehicle's target speed.

The respective reward functions are tailored to the objectives of each scenario. The reward functions for the single-lane ring and highway ramp are the average speed and throughput of the system, respectively. In the signalized intersection scenario, the reward function is defined as the average speed of all vehicles alongside other factors such as stopping time, abrupt acceleration, and fuel consumption. A thorough examination of these scenarios and reward formulations is provided in Appendix E-A.

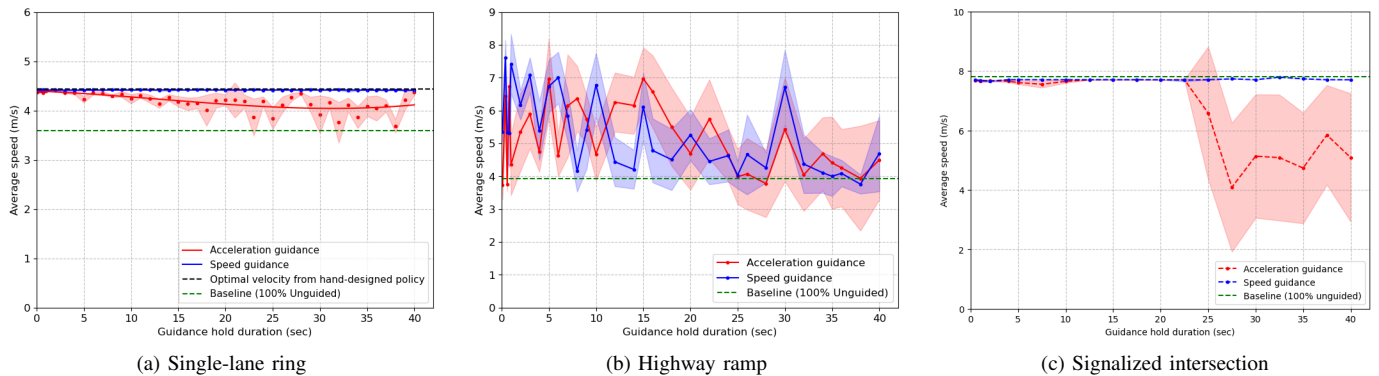


Fig. 9. System performance (average speed of all vehicles) for three traffic scenarios in mixed autonomy roadway settings. Each guidance hold duration task is trained exhaustively.

B. Experimental Setup

We utilize the microscopic traffic simulation called Simulation of Urban MObility (SUMO) [55] v.1.16.0 and its accompanying Python API, TRACI, to establish a dynamic link between our algorithmic framework and the SUMO environment. This integration is critical for implementing and testing our traffic management strategies in a controlled, simulated setting. The experiments used the MIT Supercloud with 48 CPU cores [56]. For our numerical experiments, we employed the Trust Region Policy Optimization (TRPO) algorithm [57], coupled with a Multilayer Perceptron (MLP) neural network architecture featuring two hidden layers, each with 64 units, and employing the tanh activation function. We trained and tested two different types of guidance: continuous action space for acceleration guidance and discretized action space for speed guidance. We evaluated the system’s performance over a range of guidance hold duration $\delta \in [0.1, 40]$. In our simulation experiments, we simplify the analysis by setting $\delta_{\min} = 0$, and we round the calculated δ to the nearest multiple of 10 when selecting the source training task. The detailed experimental setup is explained in Figure 8 and Appendix E-B.

C. Baselines

We compare our TTL approaches with several baselines. These baselines represent various strategies for learning and transfer in the context of coarse-grained advisory autonomy tasks.

1) *100% Unguided*: In this baseline, all vehicles are unguided, following the Intelligent Driver Model (IDM) car-following models. This scenario represents a completely decentralized system without any reinforcement learning.

2) *Oracle Transfer*: The Oracle Transfer benchmark is an idealized scenario where we train separate models for each possible source task. Once trained, we execute a zero-shot transfer by applying each model to every target task, selecting the most successful model for each.

3) *Exhaustive RL*: This strategy represents the classic approach to machine learning, where each task is trained individually and evaluated with its corresponding in-distribution trained model. The performance is evaluated by calculating the average performance across all tasks. Figure 9 illustrates the

average speed of all vehicles for three traffic networks trained exhaustively.

4) *Multitask RL*: The multitask reinforcement learning framework is designed to simultaneously train a single policy across various tasks [38], [6], here specifically by varying the guidance hold duration between 1 to 40 seconds. Each worker in the training process is assigned a specific task and contributes to a shared experience buffer. Upon completion of rollouts by all workers, the policy is updated based on the collective data in the buffer. This approach aims to explore the potential synergies and trade-offs that arise when a policy is exposed to multiple tasks during the learning process, potentially leading to more robust and generalizable policies.

5) *Random Temporal Transfer Learning (RTTL)*: Random Temporal Transfer Learning (RTTL) chooses tasks for transfer from a pool of temporal tasks at random. This scenario represents a non-deterministic transfer learning strategy and serves as a stochastic comparison point for our deterministic GTTL approach. From all the policies from the source task at each iteration, we select the top-performing one for tasks with varying hold duration. (Figure 7c)

D. Temporal Transfer Learning (TTL) results

Table II and Figure 11 illustrate the outcomes of TTL algorithms compared to baselines in different traffic environments. Here, the selected performance metric is the average speed of all vehicles evaluated in all tasks. In scenarios such as the highway ramp, while outflow is the primary reward metric, we also present the average speed as a metric for comparison. This choice is justified by the high correlation between speed and outflow, providing a consistent measure across different scenarios for a more straightforward comparative analysis. The bolded values represent the highest performance metrics achieved by TTL algorithms, discounting the Oracle Transfer due to its prohibitive computational demand. The TTL algorithms exhibit exemplary performance in both acceleration and speed guidance categories, markedly outperforming the baselines across diverse traffic conditions. Remarkably, with just a few number of source tasks, TTL algorithms approach the near-term performance of the oracle transfer. Some scenarios require a small number of source

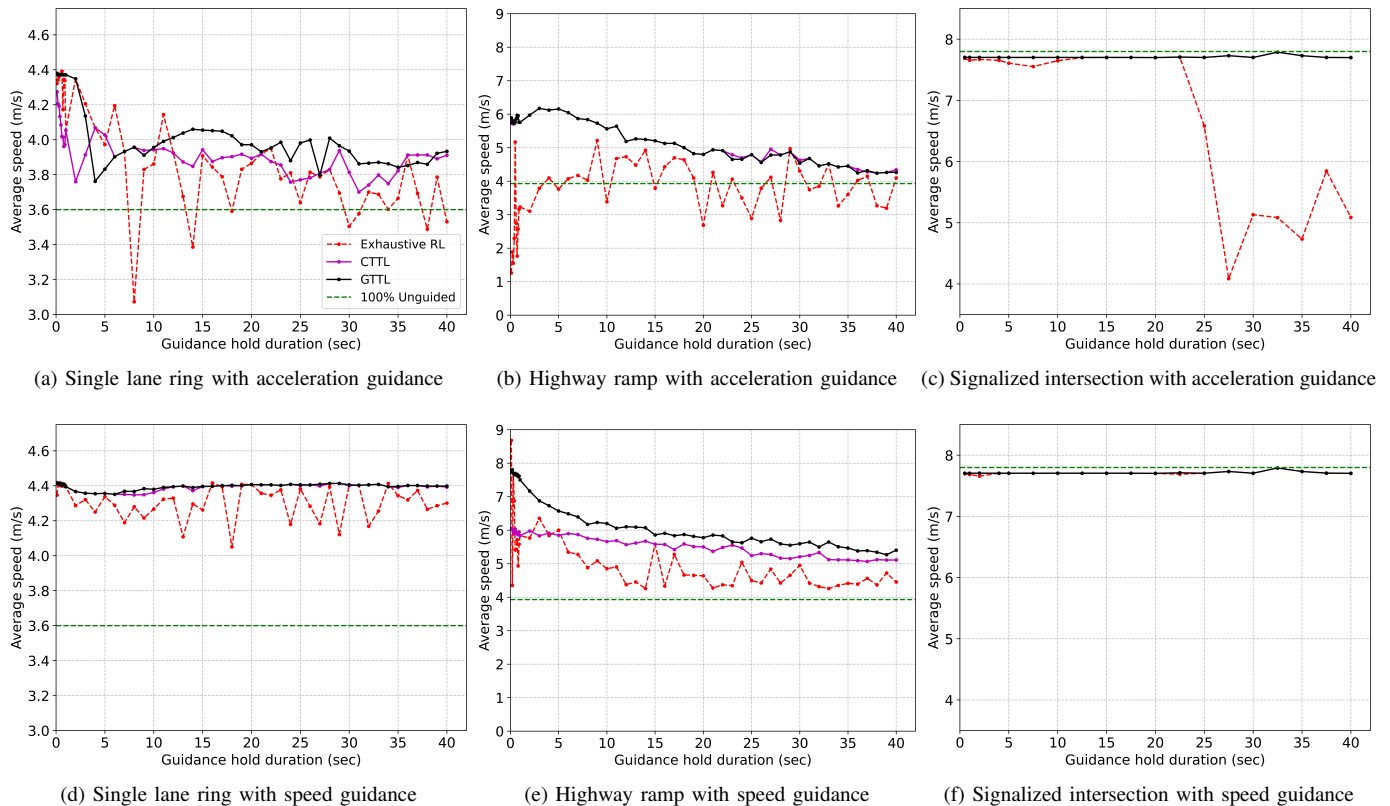


Fig. 10. System performance of Temporal Transfer Learning algorithms (GTTL and CTTL) compared to the exhaustive RL. The advisory system used either acceleration or speed guidance.

TABLE II
COMPARISON OF AVERAGE SPEEDS ACHIEVED BY DIFFERENT TRAINING METHODS ACROSS VARIOUS TRAFFIC SCENARIOS AND GUIDANCE TYPES

Methods	Training Complexity	The number of source tasks k	Traffic Scenarios					
			Single-Lane Ring		Highway Ramp		Signalized Intersection	
			Accel. Guidance	Speed Guidance	Accel. Guidance	Speed Guidance	Accel. Guidance	Speed Guidance
Oracle								
Oracle Transfer	$n \times n$	n	4.10	4.41	5.48	6.30	7.71	7.71
Exhaustive RL	n	-	3.84	4.29	4.24	4.99	6.86	7.69
Baselines								
100% Unguided	0	-	3.80	3.80	3.95	3.95	6.84	6.84
Multitask RL	$n \dagger$	-	3.94	4.28	4.53	4.42	-	-
Temporal Transfer Learning (Ours)								
Coarse-to-fine Temporal Transfer Learning (CTTL)	k	5 \ddagger	3.85	4.39	4.47	5.31	7.71	7.71
	k	10 \ddagger	4.02	4.40	5.19	5.44	7.71	7.71
	k	15 \ddagger	3.92	4.39	5.20	5.56	7.71	7.71
Greedy Temporal Transfer Learning (GTTL)	k	5	3.89	4.39	5.19	5.19	7.71	7.71
	k	10	4.03	4.40	5.19	5.54	7.71	7.71
	k	15	4.04	4.40	5.19	6.25	7.71	7.71
Ablation								
Random Temporal Transfer Learning (RTTL)	k	5	3.85	4.36	4.53	5.70	7.69	7.71
	k	10	3.97	4.39	4.89	5.87	7.70	7.71
	k	15	4.01	4.39	5.09	6.03	7.71	7.71

\dagger : denotes the number of tasks used in multitask RL. It was evaluated after the same number of rollouts of training as other settings.

\ddagger : The performance of the CTTL is assessed after completing the training across a predetermined number of source tasks at budget.

tasks to achieve the near-term performance of Oracle transfer, while others demand more extensive iterations. Specifically, in the signalized intersection scenario, all Transfer Learning methods yield the top performance when paired with speed guidance. This underscores the potency of TTL in optimizing traffic management tasks, especially when harmonized with

speed guidance. Figure 10 shows the system-level performance of each task after the temporal transfer learning methods are applied compared to the exhaustive RL.

The results presented in Figure 11 offer an insightful comparison of several training methodologies in the context of coarse-grained advisory autonomy tasks in different traffic

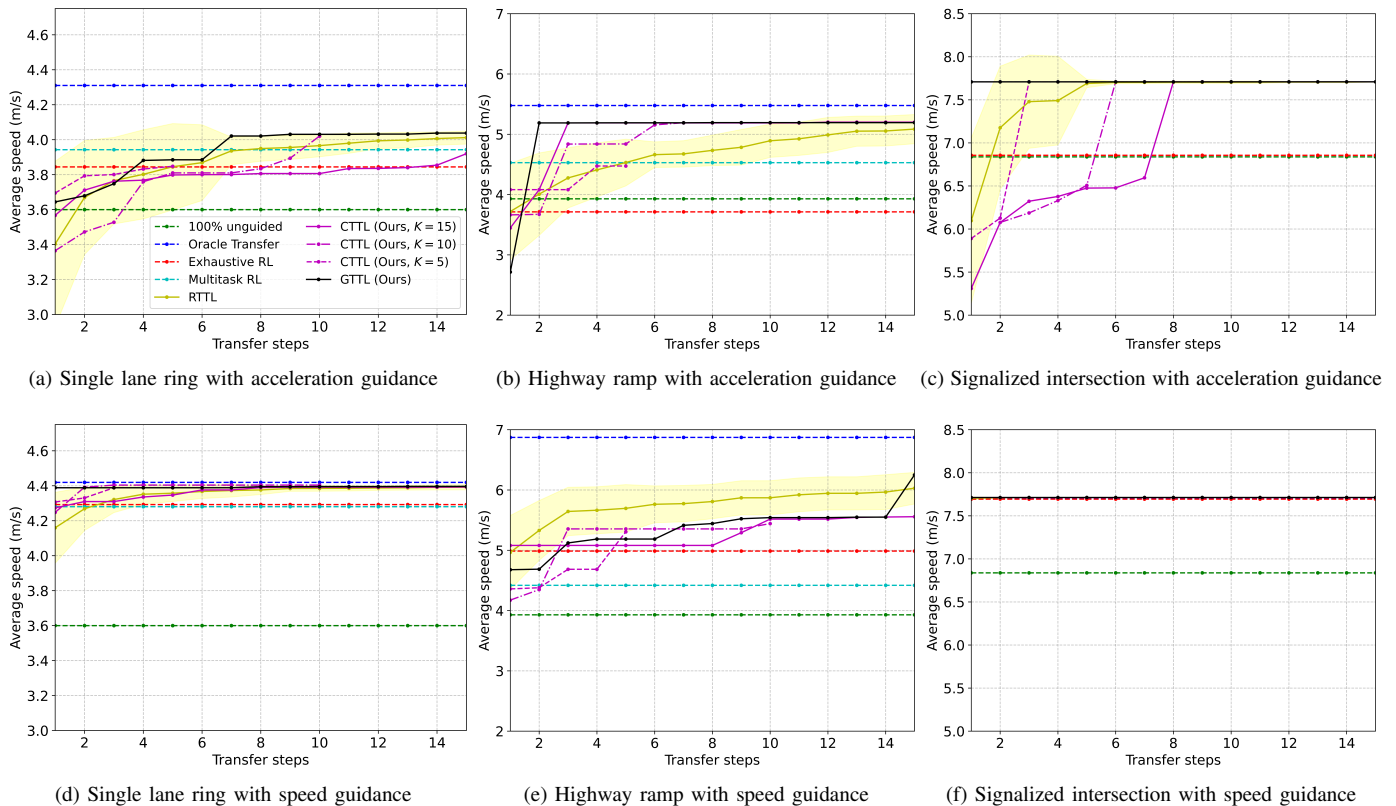


Fig. 11. System performance comparison of Temporal Transfer Learning (TTL) with various baselines in three different traffic scenarios and two different guidance types: unguided vehicles (representing a completely decentralized system), oracle transfer (showcasing zero-shot transfer capabilities), exhaustive RL (traditional separate model per task approach), multitask reinforcement learning (incorporating multiple tasks into the learning process), and transfer learning strategies such as greedy (choosing the 1-step greedy source training task) and coarse-to-fine (transferring from coarser to finer tasks progressively).

scenarios. The performance metrics present in Figure 11 indicate the average of evaluated performance across the full range of the coarse-grained advisory systems, and each task is evaluated with the average speed of all vehicles, with higher values denoting better performance. It offers a gauge for the generalizability of source tasks selected from different methods over the different target tasks.

Single-Lane Ring. Figure 9a compares the system performance of acceleration and speed guidance in the single-lane ring road network when trained from scratch. When analyzing the results, both guidance types demonstrate excellent overall performance as the guidance hold duration increases, with an average speed increase of approximately 22.22% for all vehicles in the system. However, it is worth noting that the acceleration guidance results were slightly lower than speed guidance. First, in a single-lane ring environment (Figure 11a), the average speed of GTTL starts higher than both RTTL and CTTL in the first iteration of selecting the source task. Despite a slight decrease in the early stages, the speed improves consistently over the iterations and stays competitive against the other methods. The performance of GTTL shows that it learns quickly in the initial stages and then continues to optimize its performance in subsequent steps, indicating an effective transfer of knowledge. It’s also worth noting that while no strategy surpasses Oracle Transfer’s average speed of 4.10 m/s, GTTL gets relatively close, reaching final average

speeds of approximately 4.04 m/s. While the trends for RTTL are upward as the number of source tasks gets larger, it does not exceed the performance demonstrated by GTTL. Multitask RL, although slightly surpassing the baseline, falls short when compared to our GTTL method.

Furthermore, a clear distinction is observed when comparing the number of source tasks required to achieve a given performance level across methods. To surpass baselines with exhaustive RL, RTTL necessitates approximately ten steps, whereas GTTL achieves this in merely seven steps, highlighting its efficiency. These findings strongly advocate the effectiveness of GTTL in such driving scenarios, reinforcing its potential suitability for real-world applications in achieving coarse-grained advisory systems in mixed autonomy. Upon examining speed guidance results (Figure 11d), we observe that performance levels are already near-optimal even before applying transfer learning algorithms. This observation highlights the intrinsic effectiveness of speed guidance, making the added benefits derived from implementing TTL algorithms less distinguishable in this specific scenario.

Highway Ramp. Following the single-lane ring road scenario, we analyze the results from a highway ramp scenario, where the complexity of the traffic situations and interactions are significantly elevated. Figure 9b displays the jagged performance of training exhaustively in the highway ramp road network, which could indicate the difficulty of traffic

coordination around the ramp and brittleness of RL training. However, the overall trend suggests that the average speed of all vehicles decreases as the guidance hold duration increases. In both scenarios, the multitask RL approach—trained with access to all target tasks—demonstrates a slight improvement over the unguided baseline but still falls significantly short of the performance offered by the TTL algorithms.

With the acceleration guidance (Figure 11b), Oracle Transfer, considered as upper-bound performance, consistently achieved 5.48 m/s for speed guidance, while the average speed in the unguided case is maintained around 3.95 m/s. CTTL progressively improved the average speed from 4.47 m/s within the budget of 5 to 5.20 m/s over 15 source tasks, obtaining the highest performance. GTTL started at 5.19 m/s after the first five steps, which is the highest among other methods, and eventually optimized its performance to 5.19 m/s across the 15 steps. Switching to the speed guidance scenario (Figure 11e), all methods indicated an enhancement compared to the acceleration guidance scenario. The RTTL method started at 5.70 m/s and reached a higher peak speed of 6.03 m/s. Furthermore, the CTTL method increased the average speed from 5.31 m/s to 5.56 m/s over the 15 steps. GTTL exhibited robustness, initiating at an average speed of 5.19 m/s and advancing to 6.25 m/s across the steps. This result where RTTL outperforms GTTL and CTTL highlights the unpredictable aspects of RL training, indicating that despite GTTL’s strategic framework, random task selection by RTTL can, at times, yield comparable or superior results.

Signalized Intersection. Analyzing the signalized intersection scenarios with acceleration and speed guidance reveals some notable trends. When trained exhaustively, the system performance of the signalized intersection remains steady (Figure 9c). During the training of the multitask RL policy, achieving a robust policy that could generalize across all ranges of hold duration tasks turned out to be challenging. Once the policy converged, it unfortunately led to increased collisions at intersections.

For acceleration guidance (Figure 11c), the unguided scenario and exhaustive RL resulted in average speeds of 6.84 m/s and 6.86 m/s, respectively, while Oracle Transfer reached 7.71 m/s. TTL methods, particularly CTTL and GTTL, improved significantly, up to the performance of Oracle Transfer. Speed guidance scenario (Figure 11f) benefits from the transfer learning procedures. Both CTTL and GTTL mirrored Oracle Transfer performance, achieving average speeds of around 7.71 m/s, almost close to the optimal performance. We observe that at signalized intersections with speed guidance, even a single source task allows transfer learning methods to match the performance of the oracle. This may be due to the more predictable nature of traffic dynamics at intersections, making them amenable to successful transfer with minimal learning. Moreover, the selection of the K parameter for CTTL should be strategically determined by balancing the computational budget and the complexity of the task to optimize the algorithm’s performance.

In conclusion, while unguided and exhaustive RL methods remained consistent, transfer-learning approaches showed dynamic improvements in complex traffic situations, demonstrat-

ing their potential effectiveness. This remarkable stability illustrates the robustness of the GTTL approach and its ability to deliver consistent performance, even in complex environments like signalized intersections.

VII. CONCLUSION

This paper presents temporal transfer learning (TTL) algorithms for coarse-grained advisory systems, addressing the intrinsic complexity and brittleness of RL algorithms. Through empirical analysis across three traffic scenarios, we evaluate the performance of the advisory system through either acceleration or speed and see how much performance is near-term as instantaneous control. Significant findings show that TTL outperforms baselines in diverse traffic conditions, indicating its potential to improve traffic management in mixed-autonomy environments and reduce computational cost for training RL policies. TTL algorithm is also generic and applicable to different contextual MDP tasks and can find meaningful cross-domain applications especially in industrial automation and robotics. Relaxing our initial assumptions, such as the constant estimation of training performance, could enhance our algorithm’s applicability and effectiveness. Future work will explore more complex scenarios and relax the theoretical assumptions to bridge the gap towards real-world applicability. We also underscore the potential into computationally efficient continual learning and fine-tuning strategies for transfer learning, which could offer a viable way for improved traffic management system.

APPENDIX A PROOF FOR THEOREM 1

Proof. Figure 12 illustrates the decision-making process in selecting the next hold duration δ^k that maximizes estimated performance gain within a given segment. If the segment’s performance function $J_k(\delta)$ is symmetric, the central point of the segment naturally yields the highest marginal increase in performance. Conversely, for an asymmetric $J_k(\delta)$, the selection of δ^k shifts towards one of the segment’s trisection points, dictated by the gradient of the performance function. This approach strategically expands the aggregate performance area, with each chosen δ^k representing an incremental enhancement reflected by the newly shaded region. We can divide it into three cases.

- 1) If J is symmetric,
We can divide the area into the left trapezoid and right trapezoid.

$$\begin{aligned} \max_{\delta'} (\text{Obj.}) &= \frac{1}{2}(\delta' - \delta_L)[J^* + J^* - \theta_L(\delta' - \delta_L)] \\ &\quad + \frac{1}{2}(\delta_R - \delta')[J^* - \theta_R(\delta_R - \delta') + J^*] \\ &= (\delta_R - \delta_L)J^* - \frac{\theta_L}{2}(\delta' - \delta_L)^2 \\ &\quad - \frac{\theta_R}{2}(\delta_R - \delta')^2 \end{aligned}$$

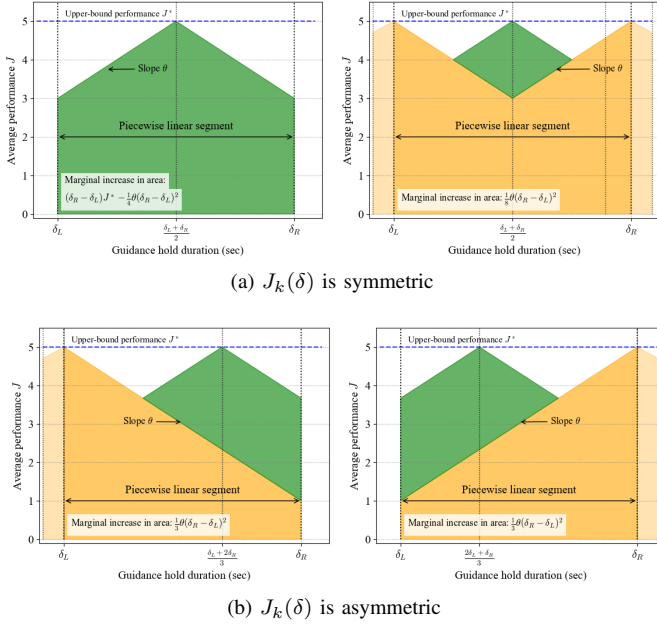


Fig. 12. Decision strategies and corresponding marginal performance increases for symmetric and asymmetric $J_k(\delta)$. (a) When $J_k(\delta)$ is symmetric about the center, the optimal δ^k coincides with the midpoint, maximizing the area under J_k . (b) For an asymmetric $J_k(\delta)$, the trisection points offer the best choice for δ^k , depending on the performance slope. The green shaded area illustrates the marginal gain achieved by selecting δ^k at the current step, contrasting with prior coverage in orange.

Find the δ' that makes $\frac{d(\text{Objective})}{d\delta'} = 0$.

$$\begin{aligned} \frac{d(\text{Objective})}{d\delta'} &= -\theta_L(\delta' - \delta_L) + \theta_R(\delta_R - \delta') = 0 \\ \delta' &= \frac{\theta_L\delta_L + \theta_R\delta_R}{\theta_L + \theta_R} \end{aligned}$$

If we assume $\theta_L = \theta_R = \theta$ (assumption 4), we get $\delta' = \frac{\delta_L + \delta_R}{2}$.

The shaded area would be as follows:

$$\begin{aligned} \sum_{\delta=\delta_L}^{\delta_R} J(\delta) &= (\delta_R - \delta_L)J^* - \frac{\theta_L}{2} \left(\frac{\delta_L + \delta_R}{2} - \delta_L \right)^2 \\ &\quad - \frac{\theta_R}{2} \left(\delta_R - \frac{\delta_L + \delta_R}{2} \right)^2 \\ &= (\delta_R - \delta_L)J^* - \theta \left(\frac{\delta_R - \delta_L}{2} \right)^2 \end{aligned}$$

Otherwise, the marginal area of increase would be calculated as follows:

$$\Delta A_k = \frac{1}{2} \left\{ \frac{1}{2}(\delta_R - \delta_L) \right\} \left\{ \frac{1}{2}\theta(\delta_R - \delta_L) \right\} = \frac{1}{8}\theta(\delta_R - \delta_L)^2.$$

2) If J has a positive slope,

$$\begin{aligned} \max_{\delta'} (\text{Obj.}) &= (\delta' - \delta_L)[J^* - (J^* - \theta(\delta_R - \delta'))] \\ &\quad + \frac{1}{2}(\delta_R + \delta')[J^* - (J^* - \theta(\delta_R - \delta'))] \\ &= (\delta' - \delta_L)\theta(\delta_R - \delta') \\ &\quad + \frac{1}{2}(\delta_R + \delta')\theta(\delta_R - \delta') \\ &= \frac{1}{2}\theta(\delta_R + 3\delta' - 2\delta_L)(\delta_R - \delta') \end{aligned}$$

Find the δ' that makes $\frac{d(\text{Obj.})}{d\delta'} = 0$.

$$\frac{d(\text{Obj.})}{d\delta'} = \frac{3}{2}\theta(\delta_R - \delta') - \frac{1}{2}\theta(\delta_R + 3\delta' - 2\delta_L) = 0$$

$$\delta_R - 3\delta' + 2\delta_L = 0$$

If we find the δ' that maximizes the area, $\delta' = \frac{2\delta_L + \delta_R}{3}$. The marginal area increase would be $\frac{1}{3}\theta(\delta_R - \delta_L)^2$.

3) If J has a negative slope, without loss of generality, δ' that maximizes the shaded area is as follows:

$$\delta' = \frac{\delta_L + 2\delta_R}{3}$$

Likewise, the marginal area increase would be $\frac{1}{3}\theta(\delta_R - \delta_L)^2$. \square

APPENDIX B PROOF FOR THEOREM 3

Proof. For the initial step,

$$\tilde{A}_1 = (\delta_{\max} - \delta_{\min})J^* - \frac{1}{4}\theta(\delta_{\max} - \delta_{\min})^2$$

For a few beginning steps, we can calculate \tilde{A}_k based on the geometric shape illustrated in fig. 6.

$$\begin{aligned} \tilde{A}_3 &= (\delta_{\max} - \delta_{\min})J^* - \frac{1}{8}\theta(\delta_{\max} - \delta_{\min})^2 \\ \tilde{A}_5 &= (\delta_{\max} - \delta_{\min})J^* - \frac{1}{16}\theta(\delta_{\max} - \delta_{\min})^2 \\ \tilde{A}_9 &= (\delta_{\max} - \delta_{\min})J^* - \frac{1}{32}\theta(\delta_{\max} - \delta_{\min})^2 \\ &\vdots \end{aligned}$$

In general, we can write a clean form of \tilde{A}_k if $k = 2^i + 1$ when $i \in \mathbb{N}$, where \mathbb{N} represents the set of natural numbers. Also, Assumption 5 leads to $J^* = \theta(\delta_{\max} - \delta_{\min})$.

$$\begin{aligned} \tilde{A}_{2^i+1} &= (\delta_{\max} - \delta_{\min})J^* - \frac{1}{2^{i+2}}\theta(\delta_{\max} - \delta_{\min})^2 \\ &= \left(1 - \frac{1}{2^{i+2}}\right)\theta(\delta_{\max} - \delta_{\min})^2 \end{aligned}$$

To cover more than $(1 - \varepsilon)(\delta_{\max} - \delta_{\min})J^*$, $2^i + 1$ steps are needed.

$$\tilde{A}_{2^i+1} \geq (1 - \varepsilon)\theta(\delta_{\max} - \delta_{\min})^2$$

$$1 - \frac{1}{2^{i+2}} \geq 1 - \varepsilon$$

$$\varepsilon \geq \frac{1}{2^{i+2}}$$

$$2^i + 1 \geq \frac{1}{4\varepsilon} + 1 = \frac{4\varepsilon + 1}{4\varepsilon}$$

To sum up, we require at least $\frac{4\varepsilon+1}{4\varepsilon}$ steps to cover more than $(1 - \varepsilon)(\delta_{\max} - \delta_{\min})J^*$. \square

APPENDIX C
PROOF FOR LEMMA 4

Proof. We prove the optimality of this CTTL algorithm under the transfer budget of K . We cut a segment of $[\delta_{\min}, \delta_{\max}]$ into $K + 1$ subsegments. We aim to maximize A_K^{CTTL} , described as the remaining area subtracted from the big rectangle of $J^*(\delta_{\max} - \delta_{\min})$. This area can be determined by aggregating the areas of the small triangles within each subsegment. The subsegments are denoted as from l_1 to l_{K+1} . The remaining area of each subsegment can be calculated as follows:

$$\begin{cases} \frac{1}{2}l_k(\theta l_k) = \frac{1}{2}\theta l_k^2 & \text{for } k = 1 \\ \frac{1}{2}l_k(\theta(\frac{1}{2}l_k)) = \frac{1}{4}\theta l_k^2 & \text{for } k = 2, \dots, K \\ \frac{1}{2}l_k(\theta l_k) = \frac{1}{2}\theta l_k^2 & \text{for } k = K + 1 \end{cases}$$

Our approach involves solving the quadratic programming problem with a linear constraint as follows:

$$\begin{aligned} \min \quad & \frac{1}{2}\theta l_1^2 + \frac{1}{4}\theta l_2^2 + \dots + \frac{1}{4}\theta l_K^2 + \frac{1}{2}\theta l_{K+1}^2 \\ \text{s.t.} \quad & l_1 + l_2 + \dots + l_K + l_{K+1} = \delta_{\max} - \delta_{\min} \\ & l_1, l_2, \dots, l_K, l_{K+1} \geq 0 \end{aligned}$$

To solve this optimization problem, we apply the Cauchy–Schwarz inequality ($\|\mathbf{u}\|\|\mathbf{v}\| \geq |\langle \mathbf{u}, \mathbf{v} \rangle|$).

$$\begin{aligned} \mathbf{u} &= \left(\frac{l_1}{\sqrt{2}}, \frac{l_2}{2}, \dots, \frac{l_K}{2}, \frac{l_{K+1}}{\sqrt{2}} \right) \\ \mathbf{v} &= (\sqrt{2}, 2, \dots, 2, \sqrt{2}) \\ \langle \mathbf{u}, \mathbf{v} \rangle &= l_1 + l_2 + \dots + l_K + l_{K+1} \\ \|\mathbf{u}\|^2 &= \left(\frac{l_1}{\sqrt{2}} \right)^2 + \left(\frac{l_2}{2} \right)^2 + \dots + \left(\frac{l_K}{2} \right)^2 + \left(\frac{l_{K+1}}{\sqrt{2}} \right)^2 \\ \|\mathbf{v}\|^2 &= \sqrt{2}^2 + 2^2 + \dots + 2^2 + \sqrt{2}^2 = 4K \\ |\langle \mathbf{u}, \mathbf{v} \rangle|^2 &= (l_1 + l_2 + \dots + l_K + l_{K+1})^2 = (\delta_{\max} - \delta_{\min})^2 \end{aligned}$$

Using the Cauchy–Schwarz inequality of $\|\mathbf{u}\| \geq \frac{|\langle \mathbf{u}, \mathbf{v} \rangle|}{\|\mathbf{v}\|}$,

$$\begin{aligned} \frac{1}{2}\theta l_1^2 + \frac{1}{4}\theta l_2^2 + \dots + \frac{1}{4}\theta l_K^2 + \frac{1}{2}\theta l_{K+1}^2 \\ &= \theta \|\mathbf{u}\|^2 \\ &\geq \theta \frac{|\langle \mathbf{u}, \mathbf{v} \rangle|^2}{\|\mathbf{v}\|^2} \\ &= \frac{\theta}{4K} (\delta_{\max} - \delta_{\min})^2 \end{aligned}$$

The equality of the Cauchy-Schwarz inequality holds when $\mathbf{u} = \lambda \mathbf{v}$.

$$\begin{aligned} \frac{l_1}{\sqrt{2}} = \frac{l_2}{2} = \dots = \frac{l_K}{2} = \frac{l_{K+1}}{\sqrt{2}} = \lambda \\ 2l_1 = l_2 = \dots = l_K = 2l_{K+1} \end{aligned}$$

Thus, the optimal solution would be as follows:

$$\begin{aligned} l_1 = l_{K+1} &= \frac{\delta_{\max} - \delta_{\min}}{2K} \\ l_2 = \dots = l_K &= \frac{\delta_{\max} - \delta_{\min}}{K}. \end{aligned}$$

Also, the optimal objective value would be $\frac{\theta}{4K} (\delta_{\max} - \delta_{\min})^2$, denoted as A_K^{CTTL} . \square

APPENDIX D
PROOF FOR THEOREM 5

Proof. We divide the case of K into $K = 2^i + 1$ and $K \neq 2^i + 1$ where $i \in \mathbb{N}$.

First, for a given K such that $K = 2^i + 1$, the relationship between A_K^{CTTL} and A_K^{GTTL} can be comprehensively understood through a detailed examination of A_K^{CTTL} and $\tilde{A}_K^{\text{GTTL}}$. These analyses are rooted in the evidence presented in the proof of theorem 3 in Appendix B.

$$\begin{aligned} A_K^{\text{CTTL}} &= \left(1 - \frac{1}{4K} \right) \theta (\delta_{\max} - \delta_{\min})^2 \\ A_K^{\text{GTTL}} &\geq \tilde{A}_K^{\text{GTTL}} = \left(1 - \frac{1}{4(K-1)} \right) \theta (\delta_{\max} - \delta_{\min})^2 \\ A_K^{\text{CTTL}} - A_K^{\text{GTTL}} &\leq A_K^{\text{CTTL}} - \tilde{A}_K^{\text{GTTL}} \\ &= \left(\frac{1}{4(K-1)} - \frac{1}{4K} \right) \theta (\delta_{\max} - \delta_{\min})^2 \\ &= \frac{1}{4K(K-1)} \theta (\delta_{\max} - \delta_{\min})^2 \end{aligned}$$

Thus, GTTL operates at a suboptimal level relative to CTTL, bounded by $\frac{1}{4K(K-1)} \theta (\delta_{\max} - \delta_{\min})^2$.

Moreover, for the case of $2^{i-1} + 1 < K < 2^i + 1$,

$$\begin{aligned} \tilde{A}_{2^i+1}^{\text{GTTL}} &= \left(1 - \frac{1}{2^{i+2}} \right) \theta (\delta_{\max} - \delta_{\min})^2 \\ \tilde{A}_{2^{i-1}+1}^{\text{GTTL}} &= \left(1 - \frac{1}{2^{i+1}} \right) \theta (\delta_{\max} - \delta_{\min})^2 \\ \tilde{A}_{2^i+1}^{\text{GTTL}} - \tilde{A}_{2^{i-1}+1}^{\text{GTTL}} &= \left(\frac{1}{2^{i+1}} - \frac{1}{2^{i+2}} \right) \theta (\delta_{\max} - \delta_{\min})^2 \end{aligned}$$

Given that all $\tilde{A}_K^{\text{GTTL}}$ where $2^{i-1} + 1 < K < 2^i + 1$ are all the same and their sum is $\left(\frac{1}{2^{i+1}} - \frac{1}{2^{i+2}} \right) \theta (\delta_{\max} - \delta_{\min})^2$, $\tilde{A}_{K+1}^{\text{GTTL}} - \tilde{A}_K^{\text{GTTL}}$ is written as follows:

$$\begin{aligned} \tilde{A}_{K+1}^{\text{GTTL}} - \tilde{A}_K^{\text{GTTL}} &= \frac{1}{(2^i + 1) - (2^{i-1} + 1)} (\tilde{A}_{2^i+1}^{\text{GTTL}} - \tilde{A}_{2^{i-1}+1}^{\text{GTTL}}) \\ &= \frac{1}{2^{2i+1}} \theta (\delta_{\max} - \delta_{\min})^2 \end{aligned}$$

$$\begin{aligned} \tilde{A}_K^{\text{GTTL}} &= \tilde{A}_{2^{i-1}+1}^{\text{GTTL}} + \frac{K - (2^{i-1} + 1)}{2^{2i+1}} \theta (\delta_{\max} - \delta_{\min})^2 \\ &= \left(1 - \frac{1}{2^{i+1}} \right) \theta (\delta_{\max} - \delta_{\min})^2 \\ &\quad + \frac{K - (2^{i-1} + 1)}{2^{2i+1}} \theta (\delta_{\max} - \delta_{\min})^2 \\ &= \left(1 - \frac{2^i}{2^{2i+1}} + \frac{K - 2^{i-1} - 1}{2^{2i+1}} \right) \theta (\delta_{\max} - \delta_{\min})^2 \\ &= \left(1 + \frac{K - 3 \cdot 2^{i-1} - 1}{2^{2i+1}} \right) \theta (\delta_{\max} - \delta_{\min})^2 \end{aligned}$$

$$\begin{aligned}
A_K^{\text{CTTL}} - A_K^{\text{GTTL}} &\leq A_K^{\text{CTTL}} - \tilde{A}_K^{\text{GTTL}} \\
&= \left(1 - \frac{1}{4K}\right) \theta(\delta_{\max} - \delta_{\min})^2 \\
&\quad - \left(1 + \frac{K - 3 \cdot 2^{i-1} - 1}{2^{2i+1}}\right) \theta(\delta_{\max} - \delta_{\min})^2 \\
&= \left(-\frac{1}{4K} - \frac{K - 3 \cdot 2^{i-1} - 1}{2^{2i+1}}\right) \theta(\delta_{\max} - \delta_{\min})^2 \\
&= \left(\frac{K - (K - 2^{i-1})(K - 2^i)}{4K \cdot 2^{2i-1}}\right) \theta(\delta_{\max} - \delta_{\min})^2 \\
&\leq \frac{1}{2^{2i+1}} \theta(\delta_{\max} - \delta_{\min})^2 \\
&\leq \frac{1}{2(K-1)^2} \theta(\delta_{\max} - \delta_{\min})^2
\end{aligned}$$

□

APPENDIX E

EXPERIMENTAL DETAILS FOR MODULAR ROAD NETWORK

A. Experiment Design

In mixed autonomy roadway settings, we investigate the traffic scenarios covered in the previous works [4], [5], [6], including the following road networks: single-lane ring, highway ramp, and signalized intersection.

a) Single-lane Ring: The single-lane circular ring road network was inspired by Sugiyama's work [58]. The single-lane ring environment aims to increase the average velocity of all vehicles in the road network. The ring circumference is 250 meters long.

The reward function is the average speed of all vehicles.

$$r(s, a) = \frac{1}{n} \sum_{\forall i} v_i(s, a) \quad (20)$$

b) Highway Ramp: The objective in the highway ramp environment was to increase the outflow given the same inflow. The reward function in the highway ramp scenario focuses on traffic flow efficiency. It is defined as the number of vehicles exiting the system. Specifically, we compare the average speed of all vehicles in the system as a performance measure.

c) Signalized Intersection: We have designed a single-lane, 4-way signalized intersection regulated by a static traffic signal phase. A multi-tasking training approach is employed to train this intersection. Specifically, we use a multi-task reinforcement learning (RL) strategy, considering various penetration rates to simulate different levels of human-guided vehicle presence. Nonetheless, when evaluating the effectiveness of this strategy, we concentrate on scenarios characterized by a penetration rate of 0.1. This allows us to assess the performance of the trained RL policy in conditions where only 10% of the vehicles are controlled by the RL policy, and the remaining 90% operate under human driving model. For the signalized intersection, the reward function incorporates multiple components to optimize various aspects of traffic flow:

$$r(s, a) = \frac{1}{n} \sum_{\forall i} v_i(s, a) - \alpha_1 \cdot P_{\text{stop}} - \alpha_2 \cdot A_{\text{accel}} - \alpha_3 \cdot F_{\text{consumption}} \quad (21)$$

where:

- P_{stop} is a penalty for vehicles stopped or moving slower than a set threshold (typically 1 m/s), aimed at reducing delays.
- A_{accel} penalizes abrupt acceleration or deceleration to encourage smoother driving.
- $F_{\text{consumption}}$ penalizes high fuel consumption, promoting eco-friendly driving practices.

The weights $\alpha_1, \alpha_2, \alpha_3$ are hyperparameters that fine-tune the significance of each penalty within the reward function, allowing for a balanced consideration of speed, safety, and efficiency based on the specific goals of each scenario. Similar to the highway ramp scenario, we compare the average speed of all vehicles in the system as a performance measure.

B. Experimental Setup

Table III states the detailed experimental setup for RL, microscopic traffic simulation, car following models, and traffic scenarios used in the experiments.

REFERENCES

- [1] C. Wu, A. Kreidieh, E. Vinitzky, and A. M. Bayen, "Emergent Behaviors in Mixed-Autonomy Traffic," in *Proceedings of the 1st Annual Conference on Robot Learning*. PMLR, Oct. 2017, pp. 398–407, iSSN: 2640-3498. [Online]. Available: <https://proceedings.mlr.press/v78/wu17a.html>
- [2] R. E. Stern, S. Cui, M. L. Delle Monache, R. Bhadani, M. Bunting, M. Churchill, N. Hamilton, R. Haulcy, H. Pohlmann, F. Wu, B. Piccoli, B. Seibold, J. Sprinkle, and D. B. Work, "Dissipation of stop-and-go waves via control of autonomous vehicles: Field experiments," *Transportation Research Part C: Emerging Technologies*, vol. 89, pp. 205–221, Apr. 2018. [Online]. Available: <https://linkinghub.elsevier.com/retrieve/pii/S0968090X18301517>
- [3] M. Sridhar and C. Wu, "Piecewise Constant Policies for Human-Compatible Congestion Mitigation," in *2021 IEEE International Intelligent Transportation Systems Conference (ITSC)*. Indianapolis, IN, USA: IEEE, Sep. 2021, pp. 2499–2505. [Online]. Available: <https://ieeexplore.ieee.org/document/9564789/>
- [4] Z. Yan and C. Wu, "Reinforcement Learning for Mixed Autonomy Intersections," in *2021 IEEE International Intelligent Transportation Systems Conference (ITSC)*, Sep. 2021, pp. 2089–2094, arXiv:2111.04686 [cs, eess]. [Online]. Available: <http://arxiv.org/abs/2111.04686>
- [5] C. Wu, A. R. Kreidieh, K. Parvate, E. Vinitzky, and A. M. Bayen, "Flow: A Modular Learning Framework for Mixed Autonomy Traffic," *IEEE Transactions on Robotics*, vol. 38, no. 2, pp. 1270–1286, Apr. 2022. [Online]. Available: <https://ieeexplore.ieee.org/document/9489303/>
- [6] Z. Yan, A. R. Kreidieh, E. Vinitzky, A. M. Bayen, and C. Wu, "Unified Automatic Control of Vehicular Systems With Reinforcement Learning," *IEEE Transactions on Automation Science and Engineering*, pp. 1–16, 2022. [Online]. Available: <https://ieeexplore.ieee.org/document/9765650/>
- [7] M. E. Taylor and P. Stone, "Transfer Learning for Reinforcement Learning Domains: A Survey," *The Journal of Machine Learning Research*, vol. 10, pp. 1633–1685, Dec. 2009.
- [8] S. J. Pan and Q. Yang, "A Survey on Transfer Learning," *IEEE Transactions on Knowledge and Data Engineering*, vol. 22, no. 10, pp. 1345–1359, Oct. 2010, conference Name: IEEE Transactions on Knowledge and Data Engineering.
- [9] A. R. Kreidieh, C. Wu, and A. M. Bayen, "Dissipating stop-and-go waves in closed and open networks via deep reinforcement learning," in *2018 21st International Conference on Intelligent Transportation Systems (ITSC)*. Maui, HI: IEEE, Nov. 2018, pp. 1475–1480. [Online]. Available: <https://ieeexplore.ieee.org/document/8569485/>
- [10] K. Jang, E. Vinitzky, B. Chalaki, B. Remer, L. Beaver, A. Malikopoulos, and A. Bayen, "Simulation to Scaled City: Zero-Shot Policy Transfer for Traffic Control via Autonomous Vehicles," Feb. 2019, arXiv:1812.06120 [cs]. [Online]. Available: <http://arxiv.org/abs/1812.06120>

TABLE III
EXPERIMENTAL PARAMETERS FOR REINFORCEMENT LEARNING, TEMPORAL TRANSFER LEARNING, SIMULATIONS, CAR FOLLOWING MODELS, AND SCENARIOS.

Type	Experiment parameters	Value
Reinforcement Learning	Training epochs	1,000
	Discount factor	0.999
	Test epochs	50
	Number of discrete action space	10
Simulation	Simulation step	0.1 s/step
	Warmup steps	500 sec
	Timestep horizon	1,000 sec
Car Following Model	Model	Intelligent Driver Model [54]
	Maximum acceleration	1 m/s ²
	Comfortable deceleration	1.5 m/s ²
	Desired velocity	30 m/s
	Minimum spacing	2 m
	Desired time headway	1 sec
	Exponent	4
Ring	Circumference	250 m
	Number of controlled vehicles	1
	Total number of vehicles	22
	Speed limit	10 m/s
Highway ramp	Mainlane inflow rate	2,000 veh/hr
	On-ramp inflow rate	300 veh/hr
	Guided vehicle penetration rate	0.1
	Speed limit	30 m/s
Signalized intersection	Inflow rate	400 veh/hr
	Signal phase time (green, red)	35, 45 sec
	Guided vehicle penetration rate	0.1
	Speed limit	14 m/s
	Weight for stop penalty	35
	Weight for acceleration	1
	Weight for fuel consumption	1
Temporal Transfer Learning	Transfer budget	15

- [11] E. Vinitzky, K. Parvate, A. Kreidieh, C. Wu, and A. Bayen, "Lagrangian Control through Deep-RL: Applications to Bottleneck Decongestion," in *2018 21st International Conference on Intelligent Transportation Systems (ITSC)*. Maui, HI: IEEE, Nov. 2018, pp. 759–765. [Online]. Available: <https://ieeexplore.ieee.org/document/8569615/>
- [12] R. Bishop, "Intelligent vehicle applications worldwide," *IEEE Intelligent Systems and their Applications*, vol. 15, no. 1, pp. 78–81, Jan. 2000, conference Name: IEEE Intelligent Systems and their Applications.
- [13] K. Katsaros, R. Kernchen, M. Dianati, and D. Rieck, "Performance study of a Green Light Optimized Speed Advisory (GLOSA) application using an integrated cooperative ITS simulation platform," in *2011 7th International Wireless Communications and Mobile Computing Conference*, Jul. 2011, pp. 918–923, iSSN: 2376-6506.
- [14] X. Xiang, K. Zhou, W.-B. Zhang, W. Qin, and Q. Mao, "A Closed-Loop Speed Advisory Model With Driver's Behavior Adaptability for Eco-Driving," *IEEE Transactions on Intelligent Transportation Systems*, vol. 16, no. 6, pp. 3313–3324, Dec. 2015, conference Name: IEEE Transactions on Intelligent Transportation Systems.
- [15] A. Hasan, N. Chakraborty, H. Chen, J.-H. Cho, C. Wu, and K. Driggs-Campbell, "PeRP: Personalized residual policies for congestion mitigation through co-operative advisory systems," in *IEEE International Conference on Intelligent Transportation Systems (ITSC)*, 2023.
- [16] B. Mok, M. Johns, K. J. Lee, D. Miller, D. Sirkin, P. Ive, and W. Ju, "Emergency, Automation Off: Unstructured Transition Timing for Distracted Drivers of Automated Vehicles," in *2015 IEEE 18th International Conference on Intelligent Transportation Systems*. Gran Canaria, Spain: IEEE, Sep. 2015, pp. 2458–2464. [Online]. Available: <http://ieeexplore.ieee.org/document/7313488/>
- [17] S. Li, R. Dong, and C. Wu, "Stabilization Guarantees of Human-Compatible Control via Lyapunov Analysis," in *2023 European Control Conference (ECC)*, Jun. 2023, pp. 1–8.
- [18] R. S. Sutton, D. Precup, and S. Singh, "Between MDPs and semi-MDPs: A framework for temporal abstraction in reinforcement learning," *Artificial Intelligence*, vol. 112, no. 1, pp. 181–211, Aug. 1999. [Online]. Available: <https://www.sciencedirect.com/science/article/pii/S0004370299000521>
- [19] A. Lakshminarayanan, S. Sharma, and B. Ravindran, "Dynamic Action Repetition for Deep Reinforcement Learning," *Proceedings of the AAAI Conference on Artificial Intelligence*, vol. 31, no. 1, Feb. 2017. [Online]. Available: <https://ojs.aaai.org/index.php/AAAI/article/view/10918>
- [20] S. Sharma, A. Srinivas, and B. Ravindran, "Learning to Repeat: Fine Grained Action Repetition for Deep Reinforcement Learning," Sep. 2020, arXiv:1702.06054 [cs]. [Online]. Available: <http://arxiv.org/abs/1702.06054>
- [21] A. Biedenkapp, R. Rajan, F. Hutter, and M. Lindauer, "TempoRL: Learning When to Act," in *Proceedings of the 38th International Conference on Machine Learning*. PMLR, Jul. 2021, pp. 914–924, iSSN: 2640-3498. [Online]. Available: <https://proceedings.mlr.press/v139/biedenkapp21a.html>
- [22] A. M. Metelli, F. Mazzolini, L. Bisi, L. Sabbioni, and M. Restelli, "Control Frequency Adaptation via Action Persistence in Batch Reinforcement Learning," in *Proceedings of the 37th International Conference on Machine Learning*. PMLR, Nov. 2020, pp. 6862–6873, iSSN: 2640-3498. [Online]. Available: <https://proceedings.mlr.press/v119/metelli20a.html>
- [23] J. Lee, B.-J. Lee, and K.-E. Kim, "Reinforcement Learning for Control with Multiple Frequencies," in *Advances in Neural Information Processing Systems*, vol. 33. Curran Associates, Inc., 2020, pp. 3254–3264. [Online]. Available: https://proceedings.neurips.cc/paper_files/paper/2020/hash/216f44e2d28d4e175a194492bde9148f-Abstract.html
- [24] L. Yang, S. Hanneke, and J. Carbonell, "A theory of transfer learning with applications to active learning," *Machine Learning*, vol. 90, no. 2, pp. 161–189, Feb. 2013. [Online]. Available: <http://link.springer.com/10.1007/s10994-012-5310-y>
- [25] M. K. Helwa and A. P. Schoellig, "Multi-robot transfer learning: A dynamical system perspective," in *2017 IEEE/RSJ International Conference on Intelligent Robots and Systems (IROS)*, Sep. 2017, pp. 4702–4708, iSSN: 2153-0866.
- [26] W. M. Kouw and M. Loog, "An introduction to domain adaptation and transfer learning," Jan. 2019, arXiv:1812.11806 [cs, stat]. [Online]. Available: <http://arxiv.org/abs/1812.11806>
- [27] N. Tripuraneni, M. Jordan, and C. Jin, "On the Theory of Transfer Learning: The Importance of Task Diversity," in *Advances in Neural Information Processing Systems*, vol. 33. Curran Associates, Inc., 2020, pp. 7852–7862. [Online]. Available: <https://proceedings.neurips.cc/paper/2020/hash/59587bffe1c7846f3e34230141556ae-Abstract.html>

- [28] J. Guan and Z. Lu, "Task Relatedness-Based Generalization Bounds for Meta Learning," in *International Conference on Learning Representations*, Jan. 2022. [Online]. Available: <https://openreview.net/forum?id=A3HHaEdqAJL>
- [29] I. Higgins, A. Pal, A. A. Rusu, L. Matthey, C. P. Burgess, A. Pritzel, M. Botvinick, C. Blundell, and A. Lerchner, "DARLA: Improving Zero-Shot Transfer in Reinforcement Learning," Jun. 2018, arXiv:1707.08475 [cs, stat]. [Online]. Available: <http://arxiv.org/abs/1707.08475>
- [30] A. A. Rusu, M. Vecerik, T. Rothörl, N. Heess, R. Pascanu, and R. Hadsell, "Sim-to-Real Robot Learning from Pixels with Progressive Nets," May 2018, arXiv:1610.04286 [cs]. [Online]. Available: <http://arxiv.org/abs/1610.04286>
- [31] A. R. Kreidieh, G. Berseth, B. Trabucco, S. Parajuli, S. Levine, and A. M. Bayen, "Inter-Level Cooperation in Hierarchical Reinforcement Learning," Nov. 2021, arXiv:1912.02368 [cs, stat]. [Online]. Available: <http://arxiv.org/abs/1912.02368>
- [32] C. K. Man, M. Quddus, and A. Theofilatos, "Transfer learning for spatio-temporal transferability of real-time crash prediction models," *Accident Analysis & Prevention*, vol. 165, p. 106511, Feb. 2022. [Online]. Available: <https://linkinghub.elsevier.com/retrieve/pii/S000145752100542X>
- [33] R. Oruche, L. Egede, T. Baker, and F. O'Donncha, "Transfer learning to improve streamflow forecasts in data sparse regions," Dec. 2021, arXiv:2112.03088 [cs]. [Online]. Available: <http://arxiv.org/abs/2112.03088>
- [34] Y. Jang, H. Lee, S. J. Hwang, and J. Shin, "Learning What and Where to Transfer," May 2019, arXiv:1905.05901 [cs, stat]. [Online]. Available: <http://arxiv.org/abs/1905.05901>
- [35] J. Sinapov, S. Narvekar, M. Leonetti, and P. Stone, "Learning Inter-Task Transferability in the Absence of Target Task Samples," in *Proceedings of the 14th International Conference on Autonomous Agents and Multi-agent Systems (AAMAS 2015)*, May 2015.
- [36] S. Li, F. Gu, G. Zhu, and C. Zhang, "Context-Aware Policy Reuse," Mar. 2019, arXiv:1806.03793 [cs] version: 4. [Online]. Available: <http://arxiv.org/abs/1806.03793>
- [37] A. Agostinelli, J. Uijlings, T. Mensink, and V. Ferrari, "Transferability Metrics for Selecting Source Model Ensembles," in *2022 IEEE/CVF Conference on Computer Vision and Pattern Recognition (CVPR)*. New Orleans, LA, USA: IEEE, Jun. 2022, pp. 7926–7936. [Online]. Available: <https://ieeexplore.ieee.org/document/9878724/>
- [38] F. Belletti, D. Haziza, G. Gomes, and A. M. Bayen, "Expert Level Control of Ramp Metering Based on Multi-Task Deep Reinforcement Learning," *IEEE Transactions on Intelligent Transportation Systems*, vol. 19, no. 4, pp. 1198–1207, Apr. 2018. [Online]. Available: <http://ieeexplore.ieee.org/document/8011495/>
- [39] X.-S. Wei, C.-L. Zhang, L. Liu, C. Shen, and J. Wu, "Coarse-to-fine: A RNN-based hierarchical attention model for vehicle re-identification," Dec. 2018, arXiv:1812.04239 [cs]. [Online]. Available: <http://arxiv.org/abs/1812.04239>
- [40] Y. Wang, R. Liu, D. Lin, D. Chen, P. Li, Q. Hu, and C. L. P. Chen, "Coarse-to-Fine: Progressive Knowledge Transfer-Based Multitask Convolutional Neural Network for Intelligent Large-Scale Fault Diagnosis," *IEEE Transactions on Neural Networks and Learning Systems*, vol. 34, no. 2, pp. 761–774, Feb. 2023, conference Name: IEEE Transactions on Neural Networks and Learning Systems.
- [41] A. Hasan, N. Chakraborty, C. Wu, and K. Driggs-Campbell, "Towards Co-operative Congestion Mitigation," Feb. 2023, arXiv:2302.09140 [cs]. [Online]. Available: <http://arxiv.org/abs/2302.09140>
- [42] C. C. Macadam, "Understanding and Modeling the Human Driver," *Vehicle System Dynamics*, vol. 40, no. 1-3, pp. 101–134, Jan. 2003. [Online]. Available: <http://www.tandfonline.com/doi/abs/10.1076/vesd.40.1.101.15875>
- [43] M. Bando, K. Hasebe, A. Nakayama, A. Shibata, and Y. Sugiyama, "Dynamical model of traffic congestion and numerical simulation," *Physical Review E*, vol. 51, no. 2, pp. 1035–1042, Feb. 1995. [Online]. Available: <https://link.aps.org/doi/10.1103/PhysRevE.51.1035>
- [44] Y. Sugiyama, "Optimal velocity model for traffic flow," *Computer Physics Communications*, vol. 121-122, pp. 399–401, Sep. 1999. [Online]. Available: <https://linkinghub.elsevier.com/retrieve/pii/S0010465599003665>
- [45] X. J. Liang, S. I. Guler, and V. V. Gayah, "Joint Optimization of Signal Phasing and Timing and Vehicle Speed Guidance in a Connected and Autonomous Vehicle Environment," *Transportation Research Record: Journal of the Transportation Research Board*, vol. 2673, no. 4, pp. 70–83, Apr. 2019. [Online]. Available: <http://journals.sagepub.com/doi/10.1177/0361198119841285>
- [46] S. Liu, W. Zhang, X. Wu, S. Feng, X. Pei, and D. Yao, "A simulation system and speed guidance algorithms for intersection traffic control using connected vehicle technology," *Tsinghua Science and Technology*, vol. 24, no. 2, pp. 160–170, Apr. 2019. [Online]. Available: <https://ieeexplore.ieee.org/document/8595295/>
- [47] X. Ma, X. Hu, S. Schweig, J. Pragalathan, and D. Schramm, "A Vehicle Guidance Model with a Close-to-Reality Driver Model and Different Levels of Vehicle Automation," *Applied Sciences*, vol. 11, no. 1, p. 380, Jan. 2021. [Online]. Available: <https://www.mdpi.com/2076-3417/11/1/380>
- [48] Z. Wang, M. Abdel-Aty, L. Yue, J. Zhu, O. Zheng, and M. H. Zaki, "Investigating the Effects of Human-Machine Interface on Cooperative Driving Using a Multi-Driver Co-Simulation Platform," *IEEE Transactions on Intelligent Vehicles*, pp. 1–14, 2023, conference Name: IEEE Transactions on Intelligent Vehicles.
- [49] F. Mannering, "An empirical analysis of driver perceptions of the relationship between speed limits and safety," *Transportation Research Part F: Traffic Psychology and Behaviour*, vol. 12, no. 2, pp. 99–106, Mar. 2009. [Online]. Available: <https://www.sciencedirect.com/science/article/pii/S1369847808000752>
- [50] V. Jayawardana, C. Tang, S. Li, D. Suo, and C. Wu, "The Impact of Task Underspecification in Evaluating Deep Reinforcement Learning," in *Advances in Neural Information Processing Systems*, S. Koyejo, S. Mohamed, A. Agarwal, D. Belgrave, K. Cho, and A. Oh, Eds., vol. 35. Curran Associates, Inc., 2022, pp. 23 881–23 893. [Online]. Available: https://proceedings.neurips.cc/paper_files/paper/2022/file/96ca792fddef7c1e3366c405022463cb-Paper-Conference.pdf
- [51] H. Wang, S. Zheng, C. Xiong, and R. Socher, "On the Generalization Gap in Reparameterizable Reinforcement Learning," in *Proceedings of the 36th International Conference on Machine Learning*. PMLR, May 2019, pp. 6648–6658, iSSN: 2640-3498. [Online]. Available: <https://proceedings.mlr.press/v97/wang19o.html>
- [52] C. Benjamins, T. Eimer, F. Schubert, A. Mohan, S. Döhler, A. Biedenkapp, B. Rosenhahn, F. Hutter, and M. Lindauer, "Contextualize Me – The Case for Context in Reinforcement Learning," *Transactions on Machine Learning Research*, Jun. 2023, arXiv:2202.04500 [cs] version: 2. [Online]. Available: <http://arxiv.org/abs/2202.04500>
- [53] J. J. Garau-Luis, Y. Miao, J. D. Co-Reyes, A. Parisi, J. Tan, E. Real, and A. Faust, "Multi-objective Evolution for Generalizable Policy Gradient Algorithms," in *Generalizable Policy Learning in the Physical World Workshop (ICLR 2022)*, 2022.
- [54] M. Treiber, A. Hennecke, and D. Helbing, "Congested Traffic States in Empirical Observations and Microscopic Simulations," *Physical Review E*, vol. 62, no. 2, pp. 1805–1824, Aug. 2000, arXiv:cond-mat/0002177. [Online]. Available: <http://arxiv.org/abs/cond-mat/0002177>
- [55] P. A. Lopez, M. Behrisch, L. Bieker-Walz, J. Erdmann, Y.-P. Flötteröd, R. Hilbrich, L. Lücken, J. Rummel, P. Wagner, and E. Wießner, "Microscopic traffic simulation using sumo," in *The 21st IEEE International Conference on Intelligent Transportation Systems*. IEEE, 2018. [Online]. Available: <https://elib.dlr.de/124092/>
- [56] A. Reuther, J. Kepner, C. Byun, S. Samsi, W. Arcand, D. Bestor, B. Bergeron, V. Gadepally, M. Houle, M. Hubbell, M. Jones, A. Klein, L. Milechin, J. Mullen, A. Prout, A. Rosa, C. Yee, and P. Michaleas, "Interactive Supercomputing on 40,000 Cores for Machine Learning and Data Analysis," in *2018 IEEE High Performance Extreme Computing Conference (HPEC)*, Sep. 2018, pp. 1–6, arXiv:1807.07814 [cs]. [Online]. Available: <http://arxiv.org/abs/1807.07814>
- [57] J. Schulman, S. Levine, P. Moritz, M. I. Jordan, and P. Abbeel, "Trust Region Policy Optimization," Apr. 2017, arXiv:1502.05477 [cs]. [Online]. Available: <http://arxiv.org/abs/1502.05477>
- [58] Y. Sugiyama, M. Fukui, M. Kikuchi, K. Hasebe, A. Nakayama, K. Nishinari, S.-i. Tadaki, and S. Yukawa, "Traffic jams without bottlenecks—experimental evidence for the physical mechanism of the formation of a jam," *New Journal of Physics*, vol. 10, no. 3, p. 033001, Mar. 2008. [Online]. Available: <https://iopscience.iop.org/article/10.1088/1367-2630/10/3/033001>